Silver/poly(vinyl alcohol)/graphene hydrogels aimed for wound dressing applications: understanding the mechanism of silver release

KATARINA NEŠOVIĆ, VESNA MIŠKOVIĆ-STANKOVIĆ*

Faculty of Technology and Metallurgy, University of Belgrade, Karnegijeva 4, 11000 Belgrade, Serbia

***Abstract*:** Long-term wound healing and chronic wound care represent significant challenges for biomaterials science and engineering with many diverse requirements for the wound dressing physico-chemical, mechanical and thermal properties, as well as antibacterial efficacy to prevent and treat persistent infections. Silver nanoparticles, as wide-spectrum antibacterial agents that do not induce bacterial resistance, are very convenient for use as an active component in antibacterial wound dressing materials with advanced properties. Polymer hydrogels have also been shown to be an excellent option as wound dressing materials, due to their many exceptional properties such as elasticity, high moisture retention ability, biocompatibility, as well as the prospect for controlled drug release. The possibility to control the release behavior of the antibacterial agent is crucially important for the efficiency of the dressing material. In this work, we aim to perform a comprehensive analysis of silver release from poly(vinyl alcohol)-based hydrogels with electrochemically synthesized antibacterial silver nanoparticles (AgNPs), aimed for wound dressing applications. Different AgNPs concentrations were loaded in hydrogel matrices and release was monitored for 28 days in physiologically-relevant conditions. The obtained experimental data were evaluated against several theoretical release models, which confirmed the predominantly diffusion-controlled mechanism of release.

***Keywords*:** silver nanoparticles; electrochemical synthesis; antibacterial biomaterials; theoretical release modeling.

***Running title*:** SILVER RELEASE FROM SILVER/POLY(VINYL ALCOHOL) HYDROGELS

INTRODUCTION

When preparing a novel biomaterial for the use in biomedical purposes there are many factors and requirements which need to be satisfied regarding the physico-chemical, mechanical and biological properties of the material [1–3]. Polymer-based wound dressings are subject of many studies because of a wide range of possibilities for tailoring their shape and form, as well as specific properties for topical applications. Poly(vinyl alcohol) is a synthetic polymer, often used in biomedicine due to its non-toxicity, solubility, biocompatibility, elasticity and the ability to form reversible hydrogels with high sorption capability [4]. In recent years, research also focuses on incorporation of graphene (Gr) in PVA

*Corresponding author. E-mail: vesna@tmf.bg.ac.rs; Tel: + 381 11 3303 687; Fax: + 381 11 3370 387

hydrogels in order to improve their mechanical strength and durability [5–7]. In clinical wound healing practieces, it is particularly important that the dressings contain anti-inflammatory and/or antibacterial active component, to protect the sterility of the wound and to prevent recurring infections and long-term inflammation of the wound area [8]. Silver nanoparticles (AgNPs) are known to possess excellent antibacterial activity, especially against some bacterial strains that are prone to developing resistance towards conventional antibiotics [9]. For that reason, AgNPs are often used as an active component in biomaterials and specifically wound dressing hydrogels based on PVA [10–19] and other polymers [20–25] that act as both carriers as well as stabilizing agents [26], preventing agglomeration of AgNPs and subsequent loss of their antibacterial properties. It is always a challenge to produce pure and stable AgNPs in polymer matrices, and there are many possible methods of synthesis, such as chemical reduction or gamma irradiation [16,27]. We have previously developed a novel electrochemical method for in situ synthesis of silver nanoparticles [12–14,28], with the advantage of simply using an ionic Ag^+ precursor ($AgNO_3$ electrolyte solution in which the hydrogels are swollen prior to the synthesis) and electrical current. The potentiostatic electrochemical reduction of Ag^+ ions to AgNPs is fast, and their properties can be controlled by varying the synthesis parameters (such as swelling time, implementation time and applied voltage) [12–14,28]. However, silver itself is also known to be toxic to some extent towards live human and animal cells [9,24,29], which is the reason why it is imperative to ensure that the produced biomaterial is not cytotoxic, and that it is safe for use.

The release behavior is a major parameter that could influence both antibacterial activity and biocompatibility, as well as the longevity of the wound dressing, therefore silver release measurements are an integral part of the *in vitro* characterizations of AgNP-loaded wound dressing materials. Generally, profiles of silver release from hydrogel matrices follow similar trends, regardless of the type of polymer and synthesis method, as they usually exhibit very quick initial release – the so-called “burst release” effect, followed by a longer period of gradual release that eventually evens out as a plateau reaching 80-100% release efficiency [11–13,28,30–35]. However, the composition and the type of the hydrogel matrix can greatly affect the rate of release and the duration of the initial burst release period [17,36–38] which could have significant implications for the antibacterial agent availability at the wound site [3], and therefore could dictate the frequency of dressing replacement. Thus, the release rate could be controlled and fine-tuned to the specific requirements for wound dressing materials, by choosing the type of polymers and designing the optimal hydrogel matrix [3,8,36,39]. An indispensable tool for release investigation and analysis is certainly modeling the experimental data with theoretical or semi-empirical equations, that could not only provide quantitative values for diffusion coefficients and other release parameters, but could also reveal the governing mechanism of release based on different theories and diffusion laws [17,40]. There are many models that can be used for evaluating the silver release profiles from polymer carriers, among which the most widespread are Korsmeyer-Peppas [41], Higuchi [42–44], Makoid-Banakar [45,46], Hixson-Crowell [42], Kopcha [47], as well as the early-time approximations [11,48–50] that are specifically used to model only the initial burst release period.

In our previous works [12–14], we have prepared and fully characterized silver/poly(vinyl alcohol) (Ag/PVA) and silver/poly(vinyl alcohol)/graphene (Ag/PVA/Gr) hydrogels, and our in vitro biological investigations [12] indicated that these materials are non-toxic and possess strong antibacterial activity. In this work, we aim to provide detailed and comprehensive study and comparison of the silver release behavior from Ag/PVA and Ag/PVA/Gr hydrogels with different AgNPs concentrations [12,13], relying on the theoretical models to gain deeper insight into the underlying phenomena and diffusion processes that govern the release rate.

EXPERIMENTAL

Material

The following chemicals were utilized for preparation of nanocomposite hydrogels: poly(vinyl alcohol) powder (fully hydrolyzed, Mw = 70–100 kDa; Sigma Aldrich, USA), silver nitrate (M. P. Hemija, Serbia), potassium nitrate (Centrohem, Serbia), graphene powder (Graphene Super-market, USA), dipotassium hydrogenphosphate, potassium dihydrogen phosphate (Sigma Aldrich, USA), sodium chloride, agar, tryptone, yeast extract (Torlak, Serbia). Ultra-pure water (18 MΩ) was obtained from the Milli-Q system (Millipore, USA) and was used in all experiments.

Synthesis of Ag/PVA and Ag/PVA/Gr nanocomposite hydrogels

The PVA and PVA/Gr hydrogels, as well as nanocomposite Ag/PVA and Ag/PVA/Gr hydrogels were prepared according to the procedure previously published elsewhere [12–14]. Briefly, 10 wt% PVA colloid dispersion was prepared by dissolving PVA powder in hot distilled water at 90 ºC for 2 h, under magnetic stirring. For PVA/Gr, graphene was added into the cooled PVA dispersion under vigorous stirring and subsequently sonicated (30 min) until uniform dispersion was obtained. The hydrogels were obtained by physical cross linking of prepared dispersions using freezing-thawing method in 5 cycles. One cycle consisted of freezing for 16 h at 18 ºC, followed by thawing for 8 h at 4 ºC. Thus obtained hydrogels were cut into discs with diameters, d, of approximately 10 mm and thickness, δ, of 5 mm. For electrochemical synthesis, the PVA and PVA/Gr hydrogel discs were immersed in $AgNO_3$ solutions of different concentrations (0.25, 0.5, 1.0 and 3.9 mM), supplemented with 0.1 M KNO_3 to improve electrical conductivity. The hydrogels were swollen at room temperature in the dark for 48 h, followed by in situ electrochemical synthesis of silver nanoparticles (AgNPs) by constant-voltage electrochemical reduction of Ag^+ ions inside the PVA and PVA/Gr polymer matrices. The hydrogel discs were placed in a special glass electrochemical cell, between working and counter electrodes (two horizontal Pt plates). The electrochemical synthesis was performed using MA 8903 Electro-Phoresis Power Supply (Iskra, Slovenia), at 90 V for 4 min, and the polarity of the electrodes was changed after the half of the implementation time, in order to dissolve the metallic silver layer formed at the hydrogel-working electrode interface. Between the experiments, the electrodes were cleaned with HNO_3 (1:1) and rinsed with distilled water. Thus obtained samples were

denoted by different names, based on the concentration of the $AgNO_3$ solution used to swell the hydrogel discs before the electrochemical synthesis, as listed in Table 1.

TABLE 1. *The adopted naming convention for the synthesized AgNP-loaded hydrogels, according to the concentrations of initial $AgNO_3$ swelling solutions used to prepare nanocomposite hydrogels*

Name of the sample	$c(AgNO_3)$ / 10^{-3} mol dm^{-3}
0.25Ag/PVA	0.25
0.25Ag/PVA/Gr	
0.5Ag/PVA	0.50
0.5Ag/PVA/Gr	
1.0Ag/PVA	1.0
1.0Ag/PVA/Gr	
3.9Ag/PVA	3.9
3.9Ag/PVA/Gr	

Physico-chemical characterizations and thermal analysis

Surface morphology of Ag/PVA and Ag/PVA/Gr hydrogels was investigated using field-emission scanning electron microscopy (FE-SEM), performed in LEO SUPRA 55 instrument (Carl Zeiss, Germany), and operated at acceleration voltage of 10 kV. The image analysis was performed using ImageJ2 (Fiji distribution) processing software [51,52].

Raman spectra of Ag/PVA and Ag/PVA/Gr were recorded on Raman spectrophotometer Renishaw Invia (Renishaw plc, UK), using a 514-nm Ar laser, in the range 3500–100 cm^{-1}.

Fourier-transform infrared (FT-IR) spectra of Ag/PVA and Ag/PVA/Gr hydrogels were collected in Spectrum one spectrophotometer (Perkin Elmer, USA). The scan was carried out in the range of 450 cm^{-1}–4000 cm^{-1} (spectral resolution of 0.5 cm^{-1}).

The thermal analyses of PVA, PVA/Gr, Ag/PVA and Ag/PVA/Gr hydrogels was carried out using a TGA Q5000 IR/SDT Q600 instrument (TA Instruments, USA), in temperature range 20–1000 °C (heating rate of 20 °C/min) under N_2 flow.

Silver release investigations

The kinetics of silver release from Ag/PVA and Ag/PVA/Gr hydrogel discs was monitored during 28 days in a modified phosphate buffered solution (PB, pH 7.4) at 37 ºC. The PB medium contained 3.9 mM KH_2PO_4 + 6.1 mM K_2HPO_4, and was modified to exclude the Cl^- ions, in order to avoid precipitation of AgCl that could affect the results of the release study. During the designated 28-day period the PB medium was changed daily for the first 7 days and ca. every 5-6 days after that (i.e., on 12th, 16th, 21st and 28th day). The amount of Ag released into the PB medium was measured using PYU UNICAM SP9 atomic absorption spectrometer (AAS) (Philips, Netherlands). Total initial amounts of Ag in the hydrogels were determined by dissolving the discs in HNO_3 (1:1 v/v) after the 28-day experiment, inducing the dissolution of all the remaining AgNPs into Ag^+. After the experimental data were

collected, several theoretical models were applied in order to discern diffusion mechanisms of silver release from the nanocomposite hydrogels.

Antibacterial activity

Antibacterial activity of PVA, PVA/Gr, Ag/PVA and Ag/PVA/Gr was evaluated for the hydrogels obtained from 0.25 mM $AgNO_3$ swelling solutions. The hydrogel samples were cut into small cubes and sterilized for 30 min in the laminar air flow hood under UV-C lamp. A Gram-positive and a Gram-negative bacterial strain was used for evaluation of antibacterial activity, namely *Staphylococcus aureus* TL (pathogenic strain, culture collection of the Faculty of Technology and Metallurgy (FTM), University of Belgrade, Serbia) and *Escherichia coli* (American Type Culture Collection (ATCC) strain no. 25922), respectively. The kinetics of the antibacterial activity was evaluated by the standard spread plate method in suspension. The number of viable bacteria colonies in the flasks containing phosphate buffer (PB), samples and bacterial culture was monitored at the beginning of the experiment and after incubation for 1, 3, and 24 h in PB at 37 ºC. After designated incubation periods, the number of viable *S. aureus* TL and *E. coli* ATCC 25922 cells was counted using a colony counter and expressed as the logarithm of the number of the colony forming units per milliliter ($\log(CFU\ ml^{-1})$).

RESULTS AND DISCUSSION

Electrochemically synthesized Ag/PVA and Ag/PVA/Gr hydrogels

The procedure of synthesis of AgNPs inside the hydrogel network has been thoroughly explained in our previous works on physicochemical and in vitro biochemical investigations of Ag/PVA and Ag/PVA/Gr hydrogels [12–14]. In brief, the hydrogels, pre-swollen in $AgNO_3$ solutions of different concentrations are placed in a two-electrode glass cell between Pt working and counter electrodes, and subjected to the constant voltage of 90 V for 4 min. During the synthesis, the reduction of Ag^+ ions and water occurs, and formation of Ag nanoparticles starts at the hydrogel/cathode interface. As bulk deposition of metallic Ag layer is undesirable at the cathode surface, the polarity of electrodes is reversed after half the implementation time, which causes anodic dissolution of bulk Ag layer. Moreover, the hydrogen that is intensively produced at the cathode due to the electrolysis of water, can permeate through the hydrogel and reduce Ag^+ ions to Ag^0 directly inside the hydrogel matrix [32,33,53], causing the formation of nucleation centers, which can further grow to form silver nanoparticles. The importance of the polymer hydrogel matrix is that it represents a stabilization agent, which favors the formation of AgNPs, limiting their agglomeration and reduces the formation of larger particles. PVA, among other polymers, is well known for its stabilizing effect on metal nanoparticles [12,54,55], which is achieved through formation of complex bonds between Ag^+ ions and lone electron pairs on the oxygen atoms of the –OH groups in PVA. These complex bonds act as anchoring sites for reduction of Ag^+ ions bound to PVA macromolecules, and for subsequent nucleation and

growth of silver nanoparticles. Thus obtained AgNPs are bound to specific sites on the PVA chains while highly porous hydrogel network lowers their surface energy and prevents agglomeration.

Fig. 1 presents FE-SEM microphotographs of Ag/PVA and Ag/PVA/Gr hydrogels. It can be seen that both hydrogels contain well-dispersed nanoparticles, whereas the average diameters were measured using the ImageJ2 software based on ≈200 nanoparticles from several micrographs. The results showed that the average AgNPs diameter was 41.86 ± 12.79 nm for Ag/PVA (average circularity 0.993) and 58.68 ± 18.53 nm for Ag/PVA/Gr (avg. circularity 0.989). Based on these results, the silver nanoparticles appear to have slightly larger dimensions in the Ag/PVA/Gr hydrogel, compared to Ag/PVA. Additionally, UV-vis spectroscopy confirmed the silver nanoparticles embedded in the Ag/PVA and Ag/PVAGr matrices, as the UV-Vis spectra exhibited peaks at 408 nm and 405 nm, respectively [12–14], proving the presence of spherical silver nanoparticles due to surface plasmon resonance effect [56,57].

FT-IR measurements were performed on PVA, PVA/Gr, Ag/PVA and Ag/PVA/Gr hydrogels in order to determine the types of bonds and interactions inside the composite hydrogels. Fig. 2 shows the characteristic fingerprint region around 1000-1700 cm^{-1} in the FTIR spectra for all hydrogel samples. The formation of complex bonds and interactions between AgNPs and –OH groups on PVA chains was confirmed for both Ag/PVA and Ag/PVA/Gr hydrogels, seen as a significant decrease in transmittance of the bands at wavenumbers 1428 cm^{-1} (C-H wagging vibrations) and 1334 cm^{-1} (coupling of the –OH in plane vibration) in the case of Ag/PVA and Ag/PVA/Gr composites compared to the pure PVA spectra. The bands around ≈1642 cm^{-1} could be ascribed to the stretching of carbonyl bonds (C=O) [58,59], and their positions did not change significantly among the different samples, although AgNPs-containing hydrogels exhibited lower transmittance compared to both PVA and (only slightly) PVA/Gr.

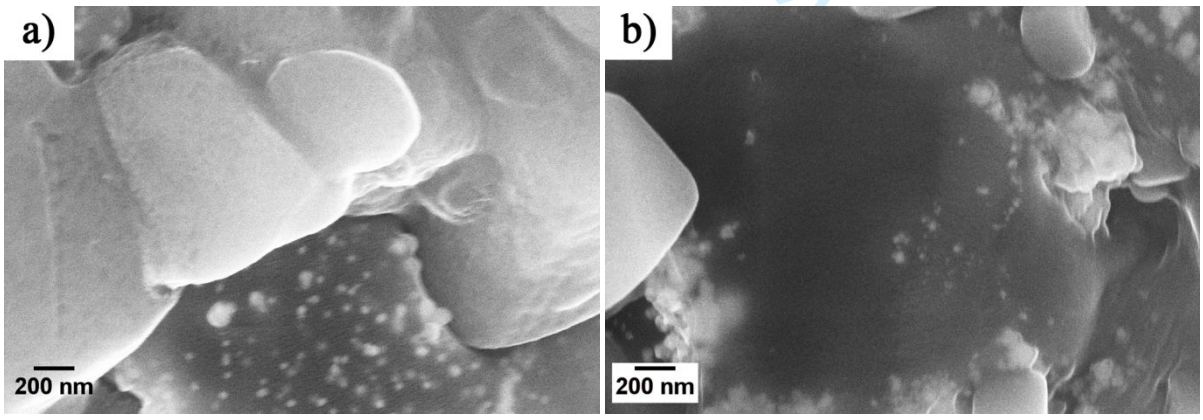

Fig. 1. FE-SEM microphotographs of a) 3.9Ag/PVA and b) 3.9Ag/PVA/Gr hydrogels

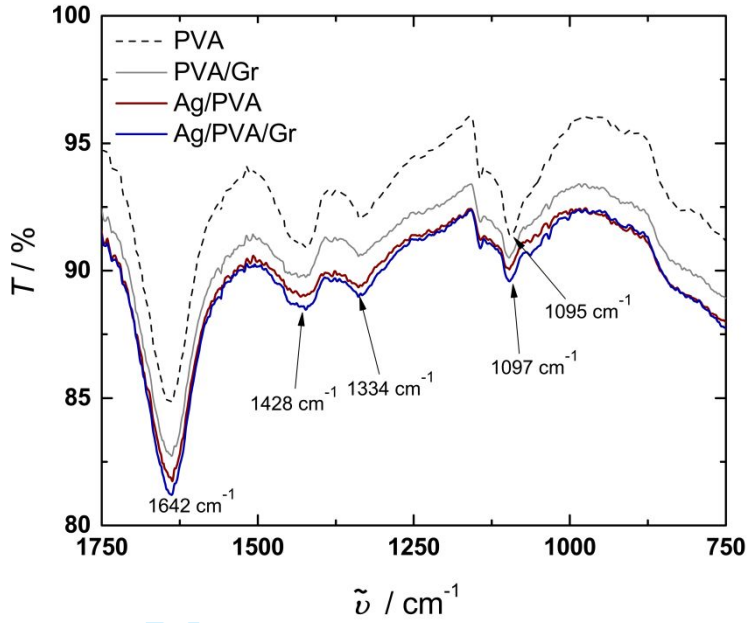

Fig. 2. The fingerprint regions of FT-IR spectra of PVA, PVA/Gr, 3.9Ag/PVA and 3.9Ag/PVA/Gr hydrogels

Raman analysis was used to confirm the incorporation of graphene sheets in PVA/Gr and Ag/PVA/Gr composite hydrogels. The presence of the graphene sheets inside the hydrogel matrices was confirmed by the appearance of two strong bands located at 1350 cm^{-1} and 1593 cm^{-1} for PVA/Gr, and at 1370 cm^{-1} and 1580 cm^{-1} for Ag/PVA/Gr (Table 2). These two peaks are characteristic of graphene structure – the first one is the D-band, which originates from the disordered carbon structure whereas the second one is the G-band, corresponding to ordered sp2-bonded carbon atoms [5]. However, the D band could also overlap with out of plane wagging vibrations of –CH_2 in poly(vinyl alcohol), which appear at similar positions ≈1370 cm^{-1} [13,60].

The differential scanning calorimetry (DSC) was used to investigate the thermal stability and phase changes occurring during the heat treatment of PVA, PVA/Gr, Ag/PVA and Ag/PVA/Gr hydrogels [14]. The characteristic DSC curves for PVA and Ag/PVA hydrogels are presented in Fig. 3, whereas the two characteristic endothermic peaks, corresponding to the temperatures of water evaporation and polymer melting, are listed in Table 2 for all investigated samples. Based on the presented data, it can be concluded that the addition of AgNPs improved the thermal stability of both silver doped hydrogels, as the first endothermic peak (corresponding to water evaporation) was found at higher temperatures for Ag/PVA and Ag/PVA/Gr (123 °C and 120 °C, respectively), in comparison to PVA and PVA/Gr (112 °C and 119 °C, respectively). The tightly bound water, consisting of highly oriented dipoles, is known to evaporate at higher temperatures [61], and the presence of AgNPs clearly contributes to the increase in the onset temperature of the water loss stage, presumably due to the ordering and orientation of H_2O dipoles inside the polymer matrix. Additionally, the presence of AgNPs caused an increase in temperature of degradation of polymer backbone of the hydrogel, as the second endothermic peak was shifted from 277 °C for PVA to 295 °C for Ag/PVA (Fig. 3), and from 287 °C for PVA/Gr to 311 °C for Ag/PVA/Gr. In addition, the second endothermic peak temperature is also shifted to higher values for

hydrogels containing graphene (277 °C and 287 °C for PVA and PVA/Gr respectively, and 295 °C and 311 °C for Ag/PVA and Ag/PVA/Gr), all leading to the conclusion that both the AgNPs and graphene significantly improved the thermal stability of polymer matrix.

TABLE 2. *The main Raman and DSC peaks ($\Delta\,\tilde{\upsilon}$ – Raman shift, T – peak temperature in the DSC curve) for PVA, PVA/Gr, 3.9Ag/PVA and 3.9Ag/PVA/Gr*

Hydrogel	$\Delta\,\tilde{\upsilon}$ / cm^{-1}		T / °C	
	D-peak	G-peak	first endothermic peak	second endothermic peak
PVA	/	/	112	277
PVA/Gr	1350	1593	119	287
3.9Ag/PVA	/	/	123	295
3.9Ag/PVA/Gr	1370	1580	120	311

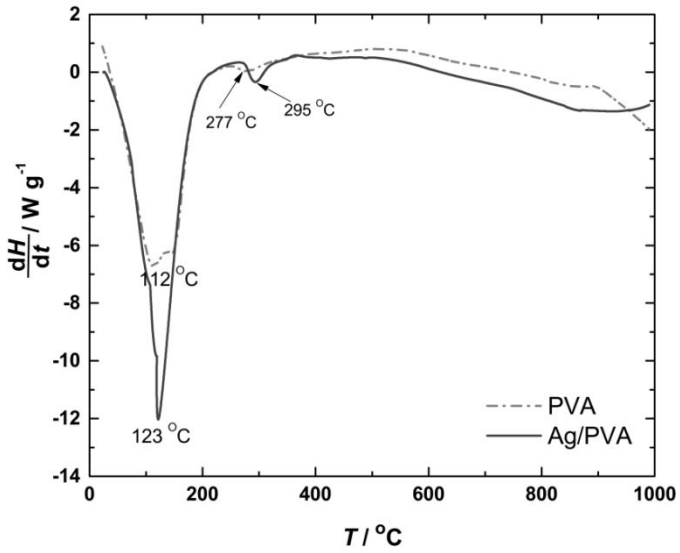

Fig. 3. DSC curves for PVA and 3.9Ag/PVA hydrogels

Silver release measurements and modeling

The kinetics of antibacterial agent release is very important for the applications of antibacterial medical devices, as it influences their antibacterial efficiency and life cycle. The release of silver nanoparticles was monitored over the time period of 28 days, and based on the obtained experimental data, it was found that, in the initial period, hydrogels exhibited „burst release," marked by a sharp decrease in Ag content, but the release profiles reached a plateau after around 2-5 days, and further release was significantly slower. Table 3 represents the obtained data for the initial concentrations of silver in the hydrogel matrices, c_0, and the remaining concentrations, $c_{Ag,rem,}$ in the hydrogel matrices after 28 days release, measured by AAS, as well as the percentages of the released silver during this 28-day period. This release behavior is especially important for wound dressings, as the high initial release of antibacterial agent to the wound and surrounding tissue ensures prevention of adhesion

of bacteria and biofilm formation. Subsequent slow and steady release can preserve the sterility of the wound and prevent infection over prolonged application period. It is obvious that all hydrogels retained a certain amount of silver in their matrices after prolonged release, attesting to their longevity as potential wound dressings. However, a high percentage (60-80 %) of the total initial amount of AgNPs was released during the monitored period, confirming that these materials could provide sustained infection protection to the wound. The results of silver release indicated that Ag/PVA and Ag/PVA/Gr hydrogels can be applied for prolonged periods, providing sufficient amount of antibacterial agent to preserve the sterility of the wound dressing or soft tissue implant.

TABLE 3. *Total initial silver concentration in all of the hydrogel samples, c_0, and the remaining concentrations, $c_{Ag,rem}$, in the hydrogel matrices after 28 days release in the PB medium at 37 °C, as well as the percentages of released silver during this release period*

hydrogel	$c_{Ag,0}$ / mg dm^{-3}	$c_{Ag,rem}$ / mg dm^{-3}	% released
0.25Ag/PVA	41.3±8.0	13.3±3.8	68
0.5Ag/PVA	50.8±7.2	26.6±2.7	48
1.0Ag/PVA	81.4±15.8	27.9±4.3	66
3.9Ag/PVA	247.5±27.9	65.4±3.4	74
0.25Ag/PVA/Gr	28.2±1.7	9.7±3.6	66
0.5Ag/PVA/Gr	64.8±5.6	28.3±7.8	56
1.0Ag/PVA/Gr	70.6±14.7	15.2±6.1	78
3.9Ag/PVA/Gr	273.1±19.5	59.4±12.2	78

The generated release profiles were fitted with several theoretical models, in order to investigate the kinetics of the silver release. The models were chosen among those most frequently found in literature to describe the diffusion mechanisms behind the drug release processes. One of these models deals with the so-called “burst release” effect that is often observed during release of drugs and other active substances from polymer carriers, and as such is used to describe the diffusion in the early phase of release, thus it is called the early time approximation (ETA). For ETA, two equations were used to compare the appropriateness of the model for our experimental data. Specifically, a widely used standard ETA (Eq. (1)) [11,48,49], and a modified ETA (Eq. (2)) proposed by Ritger and Peppas [50] were applied. In these equations, $c_{Ag,t}/c_{Ag,0}$ denotes the fraction of released silver at the time t, D_{Ag} is the diffusion coefficient of silver during the release, t – the time of release, δ is the hydrogel sample thickness and r is the radius of the hydrogel disc.

$$\frac{c_{Ag,t}}{c_{Ag,0}} = 4 \cdot \left(\frac{D_{Ag} \cdot t}{\pi \cdot r^2} \right)^{1/2} \quad (1)$$

$$\frac{c_{\mathrm{Ag,t}}}{c_{\mathrm{Ag,0}}} = 4\cdot\left(\frac{D_{\mathrm{Ag}}\cdot t}{\pi\cdot r^2}\right)^{1/2} - \pi\cdot\left(\frac{D_{\mathrm{Ag}}\cdot t}{\pi\cdot r^2}\right) - \frac{\pi}{3}\cdot\left(\frac{D_{\mathrm{Ag}}\cdot t}{\pi\cdot r^2}\right)^{3/2} + 4\cdot\left(\frac{D_{\mathrm{Ag}}\cdot t}{\pi\cdot \delta^2}\right)^{1/2} - \frac{2r}{\delta}\cdot\left[8\cdot\left(\frac{D_{\mathrm{Ag}}\cdot t}{\pi\cdot r^2}\right) - 2\pi\cdot\left(\frac{D_{\mathrm{Ag}}\cdot t}{\pi\cdot r^2}\right)^{3/2} - \frac{2\pi}{3}\cdot\left(\frac{D_{\mathrm{Ag}}\cdot t}{\pi\cdot r^2}\right)^{2}\right] \quad (2)$$

The ETA models represent the dependence of the fraction of released silver on the square root of the release time, according to both the Eq. (1) and (2); however, the Eq. (1) implies that this dependence should be linear, whereas the Eq. (2) suggests non-linear relationship for the release from thick hydrogel discs and slabs. Figs. 4 and 5 represent the ETA models for silver release from Ag/PVA and Ag/PVA/Gr hydrogels, respectively. From the obtained results, it can be observed that the modified ETA model provided much better correlation with the experimental data, which was to be expected due to the considerations of the geometry of release, as discussed above. It is also obvious that the best correlation, spanning almost the entire release periods, were achieved for hydrogels with lower AgNPs concentrations, i.e., 0.25Ag/PVA, 0.5Ag/PVA (Figs. 4a and 4b), 0.25Ag/PVA/Gr and 0.5Ag/PVA/Gr (Figs. 5a and 5b). On the other hand, hydrogels with higher amounts of silver (1.0Ag/PVA, 3.9Ag/PVA (Figs. 4c and 4d), 1.0Ag/PVA/Gr and 3.9Ag/PVA/Gr (Figs. 5c and 5d)), exhibited narrower timespan over which the ETA model could be applied, which could be due to the fact that the burst release effect was much more pronounced for these hydrogels – more than 60 % of silver was released within the first 48 h. The quantitative results for the diffusion coefficients, D_{Ag}, of silver from the hydrogel matrices, calculated from both the standard and modified ETA models, are listed in Table 4. The obtained D_{Ag} data provide another interesting observation, that the values calculated by the standard ETA models are always significantly higher than the corresponding D_{Ag} values from the modified ETA fit. This implies that the standard ETA model usually overestimates the rate of drug release from cylindrical samples, and thus it should be used with caution, and replaced with the modified model whenever possible.

TABLE 4. *Diffusion coefficients, D_{Ag}, of silver from the hydrogel matrices, calculated from the standard and modified ETA models*

	Standard ETA	Modified ETA
sample	D_{Ag} / 10^{-8} cm^2 s^{-1}	D_{Ag} / 10^{-8} cm^2 s^{-1}
0.25Ag/PVA	1.60	0.53
0.5Ag/PVA	1.40	0.38
1.0Ag/PVA	6.79	2.75
3.9Ag/PVA	12.7	5.92
0.25Ag/PVA/Gr	1.71	0.49
0.5Ag/PVA/Gr	1.40	0.53
1.0Ag/PVA/Gr	10.9	4.38
3.9Ag/PVA/Gr	15.6	7.07

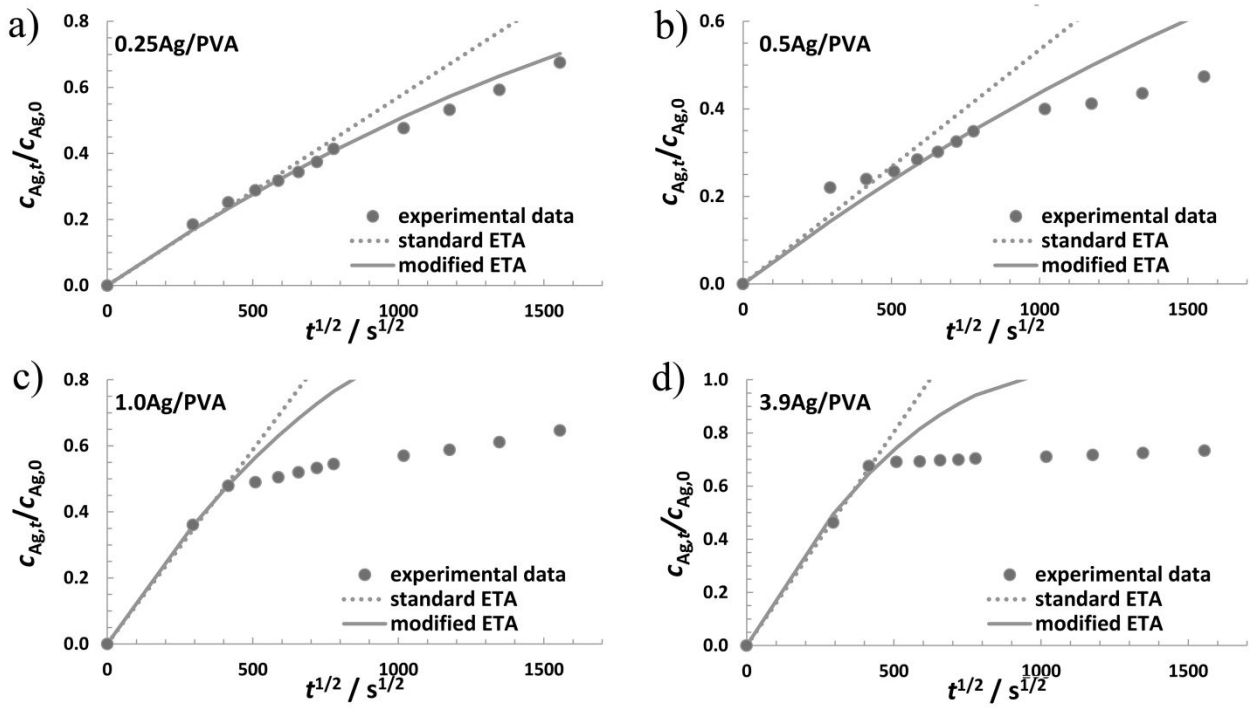

Fig. 4. Early time approximations (ETA) for silver release from a) 0.25Ag/PVA, b) 0.5Ag/PVA, c) 1.0Ag/PVA, and d) 3.9Ag/PVA hydrogels

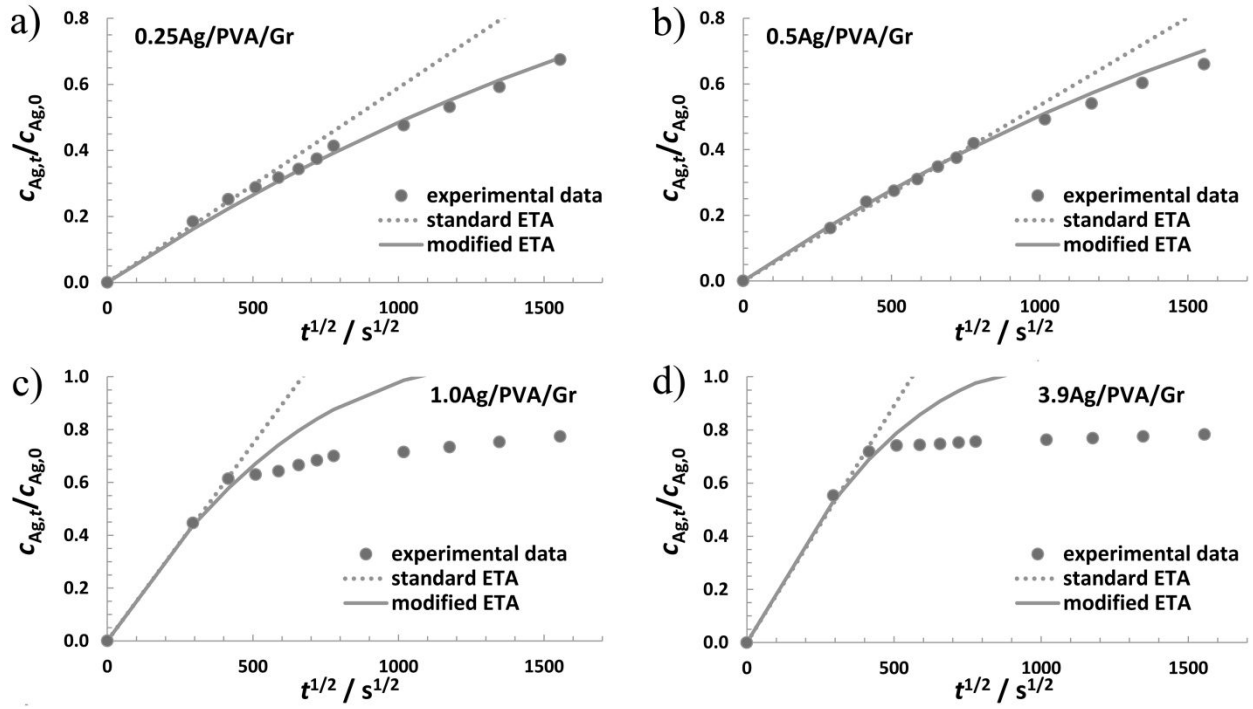

Fig. 5. Early time approximations (ETA) for silver release from a) 0.25Ag/PVA/Gr, b) 0.5Ag/PVA/Gr, c) 1.0Ag/PVA/Gr, and d) 3.9Ag/PVA/Gr hydrogels

Further, another three theoretical models were applied to the release data, in order to elucidate the diffusion parameters over the entire release period, and to quantitatively compare silver release behavior of different hydrogels. The models applied were Makoid-Banakar [45,46], Korsmeyer-Peppas [41] and Kopcha [47], which are described by equations (3), (4) and (5), respectively.

$$\frac{c_{\mathrm{Ag,t}}}{c_{\mathrm{Ag,0}}} = k_{\mathrm{MB}} \cdot t^{\mathrm{n}} \cdot \exp\left(-c \cdot t\right) \tag{3}$$

$$\frac{c_{\mathrm{Ag,t}}}{c_{\mathrm{Ag,0}}} = k_{\mathrm{KP}} \cdot t^{\mathrm{n}} \tag{4}$$

$$\frac{c_{\mathrm{Ag,t}}}{c_{\mathrm{Ag,0}}} = A \cdot t^{1/2} + B \cdot t \tag{5}$$

The meanings of physical quantities and constants in equations (3), (4) and (5) are: $c_{Ag,t}$ – concentration of Ag released at time t; $c_{Ag,0}$ – initial concentration of Ag in the hydrogel before release; k_{MB} – Makoid-Banakar constant; c – Makoid-Banakar parameter (related to dissolution limitations as the function approaches maximum value); k_{KP} – Korsmeyer-Peppas constant; n – coefficient which describes release transport mechanism (n < 0.5 – Fickian diffusion, n > 0.5 – non-Fickian/anomalous diffusion, n = 1 – Case II transport [41]); A and B – Kopcha's constants which depend on the dominant transport phenomena during release.

The release profiles, representing the dependence of the fraction of released silver, $c_{Ag,t}/c_{Ag,0}$, on the time of release, t, for 0.25Ag/PVA, 0.5Ag/PVA, 1.0Ag/PVA and 3.9Ag/PVA, as well as for 0.25Ag/PVA/Gr, 0.5Ag/PVA/Gr, 1.0Ag/PVA/Gr and 3.9Ag/PVA/Gr hydrogels, are presented in Figs. 6 and 7, respectively. Additionally, the values for different fit parameters and constants for all three models are listed in the Table 5. Analyzing the experimental release profiles, the first observation is that the hydrogels with higher AgNPs contents (1.0Ag/PVA, 3.9Ag/PVA, 1.0Ag/PVA/Gr and 3.9Ag/PVA/Gr) exhibited very quick initial release within the first 48 h or so, corresponding with the so-called "burst" effect that was also noticed during fitting with early time approximations. From Figs. 6b,d,f and 7b,d,f, it could be concluded that the burst effect resulted in the release of ≈50 % of the initial silver concentration, for the hydrogels obtained from 1.0 mM $AgNO_3$ swelling solutions, i.e., nearly 70 % in the case of hydrogels obtained from 3.9 mM $AgNO_3$ swelling solutions. The hydrogels with lower AgNPs concentrations, also exhibited the burst effect, but in those cases it was noted as the release of ≈20 % of silver within the initial 24 h, which was followed by more gradual release, and the release rate consistently slowed down towards the end of the monitored 28-day period. The more gradual release from hydrogels with lower AgNP contents also resulted in better overall correlation of all models with the experimental data, compared to the hydrogels obtained from 1.0 mM and 3.9 mM $AgNO_3$ swelling solutions that could be observed both visually in Figs. 6 and 7, as well as through the values of the coefficient of determination, R^2 (Table 5), which provides a measure of how well the models correspond to the experimental data, and which was always higher for hydrogels obtained from 0.25 mM and 0.5 mM $AgNO_3$ solutions, often even >0.99.

Comparing different models amongst themselves, the Korsmeyer-Peppas and the Makoid-Banakar models provided notably better correlation with the experimental data, compared to the Kopcha model, which was especially pronounced in the case of hydrogels with higher silver contents. On the other hand, the Korsmeyer-Peppas and the Makoid-Banakar models did not differ significantly, which was not surprising, as the Korsmeyer-Peppas model (Eq. (4)) can be seen as an approximation of the Makoid-Banakar equation (Eq. (3)), in the edge case when $c \to 0$. From Table 5, it is obvious that the *c* parameter from the Makoid-Banakar model was indeed very small, indicating that the Makoid-Banakar and Korsmeyer-Peppas models were very similar for AgNP-loaded hydrogels, which was further confirmed by the fact that parameters n, as well as k_{KP} and k_{MB} constants had very similar values. As already mentioned, the time exponent n is an indication of the dominant diffusion mechanism, and, as its values were always <0.5 (Table 5), it can be concluded that the release of silver from all of the hydrogels conformed to the Fickian diffusion behavior [41] and was governed mainly by the concentration gradient of released silver. This was also confirmed by the Kopcha models, as the absolute values of the parameter A were higher compared to |B|, indicating that the predominant driving force for the release is the diffusion, and not the polymer matrix relaxation [11].

Another quite well-known and widely used model, namely the Higuchi model [43,62], was also applied in order to compare it with other models and to gain insight into the governing phenomena during release. The Higuchi model is based on several assumptions for the derivation of the mathematical model, including time- and concentration-independent diffusion coefficients, perfect sink conditions, steady-state release, insolubility of the carrier matrix, one-dimensional geometry, as well as the condition that the initial concentration of the drug is significantly greater than its solubility in the release medium [43,62,63]. The mathematical expression for the Higuchi model (Eq. (6)) is quite simple and equivalent to the aforementioned standard ETA model (Eq. (1)), as they both imply the linear dependence of the fraction of released drug and square root of time, although the proportionality constant, the so-called Higuchi constant, k_H, has slightly different meaning than in the ETA model [44]. Based on these considerations, it could be anticipated that the Higuchi model would not provide appropriate description of silver release from the investigated Ag/PVA and Ag/PVA/Gr hydrogels, as some of the basic assumptions are too simplified for the given system, most important of which is neglecting the radial diffusion of silver along the hydrogel edges. Thus, as expected, Fig. 8 reveals that the Higuchi equation is appropriate only in the initial period of release, whereas this model significantly overestimates the amount of released silver during prolonged exposure to PB, much like the standard ETA model in Figs. 4 and 5. It could be also noticed that the Higuchi model agrees better with the experimental data for hydrogels with lower AgNPs concentrations (obtained from 0.25 and 0.5 mM swelling solutions), whereas the correlation holds only for the first two days in the case of 1.0 and 3.9 mM hydrogels. This is most probably the consequence of the fact that the latter hydrogels release drastically higher fraction of silver within the first 48 h (up to 50-70%), whereas for 0.25 and 0.5 mM hydrogels, only ≈40% is released over the course of 12 days, as discussed above.

$$\frac{c_{\mathrm{Ag,t}}}{c_{\mathrm{Ag,0}}} = k_{\mathrm{H}} \cdot t^{1/2} \qquad (6)$$

TABLE 5. *Fitting parameters obtained from Korsmeyer-Peppas, Makoid-Banakar and Kopcha models of silver release from the hydrogel matrices*

	Korsmeyer-Peppas			Makoid-Banakar				Kopcha		
hydrogel	k_{KP} / s^{-n}	**n**	R^2	k_{MB} / s^{-n}	**n**	**c / 10^{-7} s^{-1}**	R^2	**A / 10^{-3} $s^{-1/2}$**	**B / 10^{-7} s^{-1}**	R^2
0.25Ag/PVA	0.003	0.376	0.998	0.003	0.376	0.000034	0.998	0.61	-1.24	0.995
0.5Ag/PVA	0.012	0.251	0.994	0.011	0.261	0.12	0.994	0.61	-2.06	0.970
1.0Ag/PVA	0.087	0.136	0.987	0.055	0.174	0.51	0.989	1.12	-4.83	0.896
3.9Ag/PVA	0.247	0.077	0.946	0.070	0.182	1.49	0.967	1.56	-7.45	0.846
0.25Ag/PVA/Gr	0.002	0.389	0.996	0.001	0.462	0.81	0.9983	0.61	-1.20	0.998
0.5Ag/PVA/Gr	0.010	0.276	0.971	0.002	0.419	1.72	0.986	0.72	-2.44	0.985
1.0Ag/PVA/Gr	0.137	0.120	0.976	0.053	0.199	1.08	0.986	1.45	-6.50	0.901
3.9Ag/PVA/Gr	0.316	0.064	0.970	0.118	0.146	1.17	0.983	1.69	-8.14	0.826

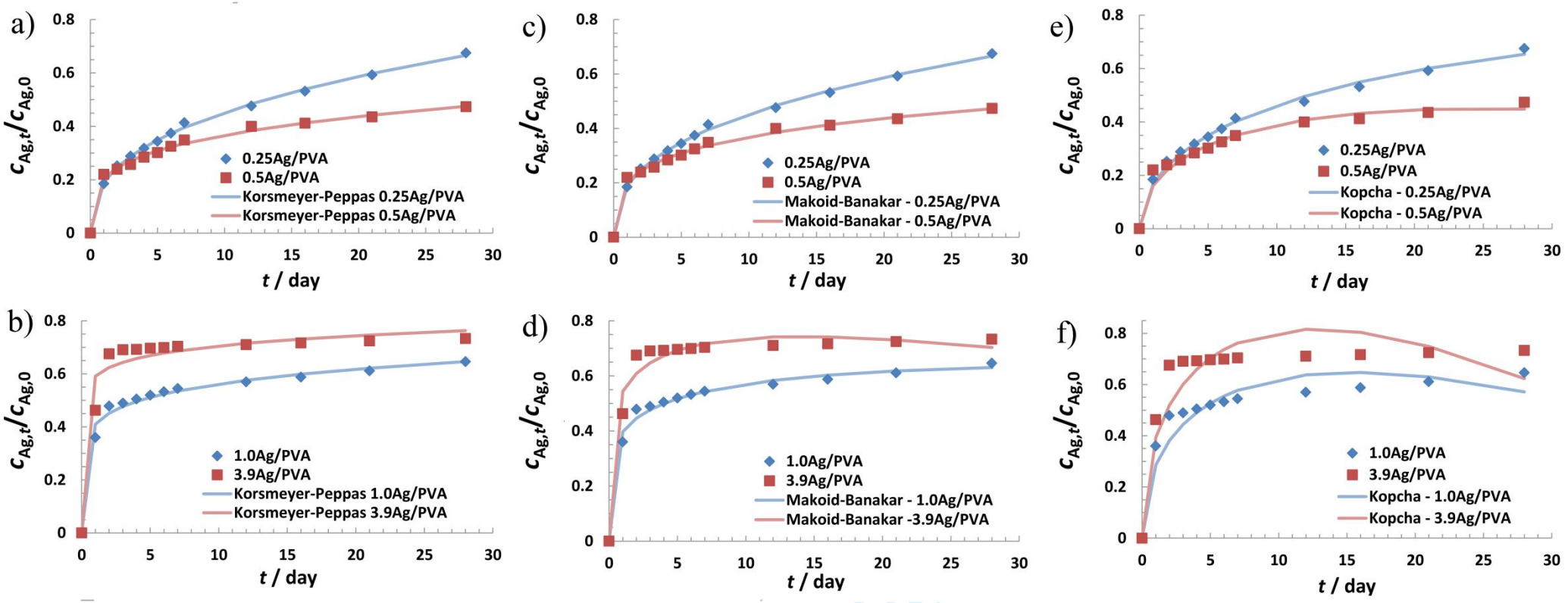

Fig. 6. Models of silver release from 0.25Ag/PVA, 0.5Ag/PVA, 1.0Ag/PVA, and 3.9Ag/PVA hydrogels: a) and b) Korsmeyer-Peppas, c) and d) Makoid-Banakar, e) and f) Kopcha

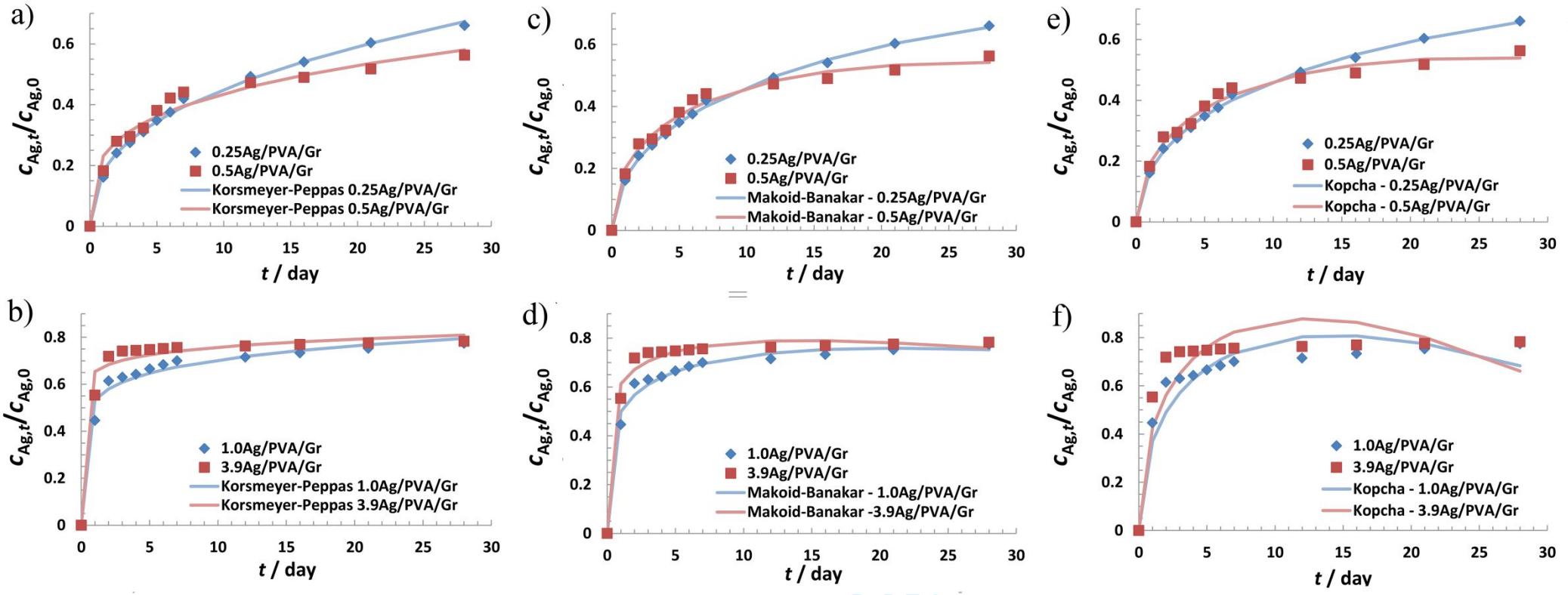

Fig. 7. Models of silver release from 0.25Ag/PVA/Gr, 0.5Ag/PVA/Gr, 1.0Ag/PVA/Gr, and 3.9Ag/PVA/Gr hydrogels: a) and b) Korsmeyer-Peppas, c) and d) Makoid-Banakar, e) and f) Kopcha

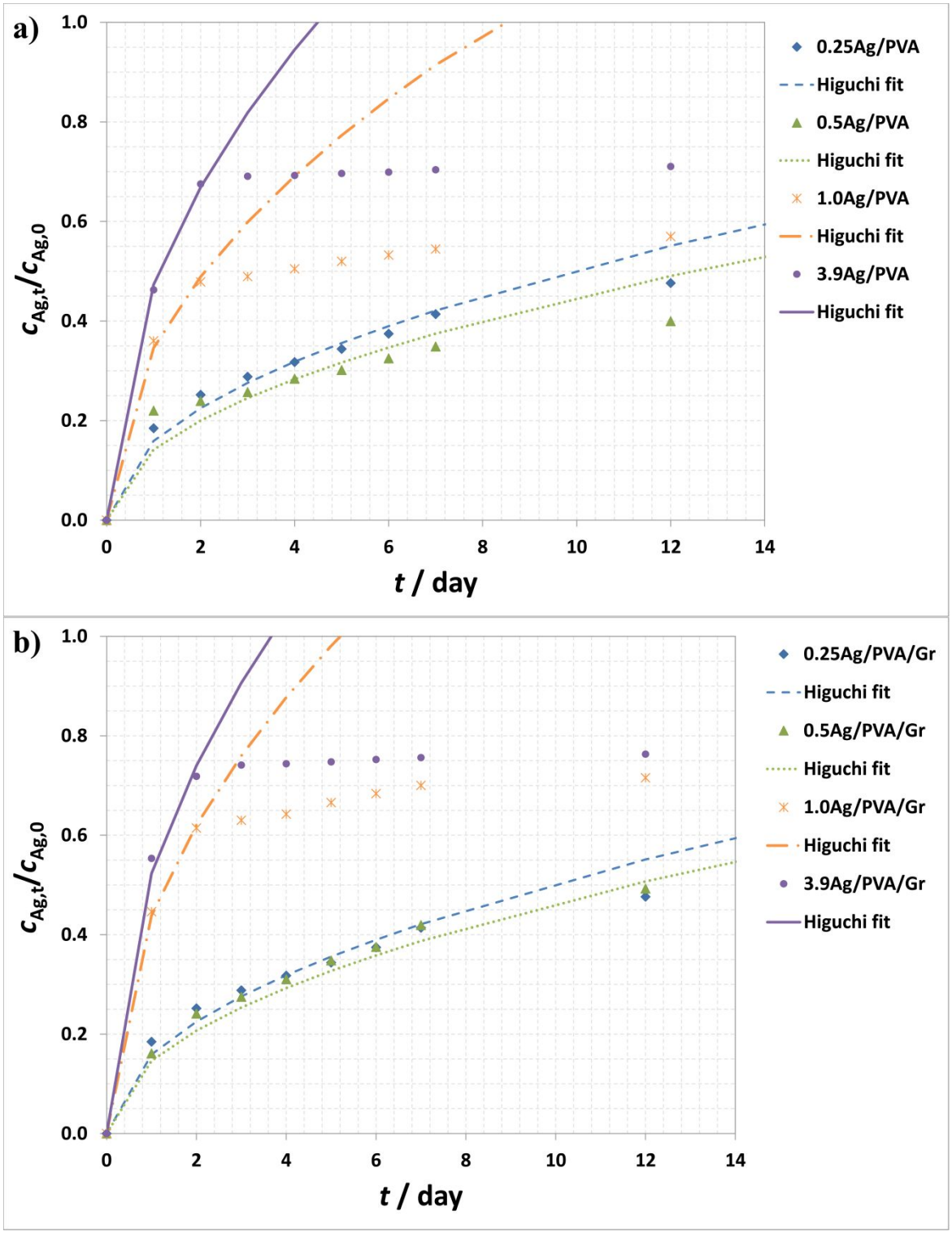

Fig. 8. Higuchi models for a) Ag/PVA and b) Ag/PVA/Gr hydrogels with different AgNPs concentrations

Antibacterial activity

The antibacterial activity kinetics of 0.25Ag/PVA and 0.25Ag/PVA/Gr hydrogel discs was investigated against *Staphylococcus aureus* TL and *Escherichia coli* ATCC25922 bacterial strains, using the spread-plate method in suspension. The samples and bacteria were incubated in phosphate buffer (PB) at 37 °C for 1 h, 3 h and 24 h, after which the colonies were seeded on agar base and counted using a colony counter. Fig. 9 represents the photographs of colonies on the agar base in a Petri dish, immediately after the inoculation and after incubation for 1 h with the 0.25Ag/PVA/Gr hydrogel. Even after 1 h, both hydrogels exhibited strong antibacterial activity, with 0.25Ag/PVA causing 44.8 % reduction of *S. aureus* TL and 100 % reduction of *E. coli* ATCC25922 [12,14]. Similarly, the 0.25Ag/PVA/Gr caused 97 % and 100 % reduction of *S. aureus* TL and *E. coli* ATCC25922, respectively [12,14]. Obviously, the 0.25Ag/PVA/Gr exhibited stronger antibacterial activity after 1 h of incubation, however, both samples caused total reduction of both *S. aureus* TL and *E. coli* ATCC25922 colonies after only 3 h of incubation [12]. Clear correlation between the hydrogels' antibacterial effect and the release profiles could be observed, as the very quick bacteria eradication within 1-3 h is probably a consequence of the burst silver release effect, depicted in releasing up to 20-40 % of the initial AgNPs concentration from the hydrogels within the initial 1-day period. Considering that the nanocomposite hydrogels were synthesized from the swelling solutions of the lowest $AgNO_3$ concentration (0.25 mM), these findings confirm that 0.25Ag/PVA and 0.25Ag/PVA/Gr have good potential for the use as antibacterial biomedical devices even with low amounts of incorporated AgNPs, which reduces the potential cytotoxicity risk.

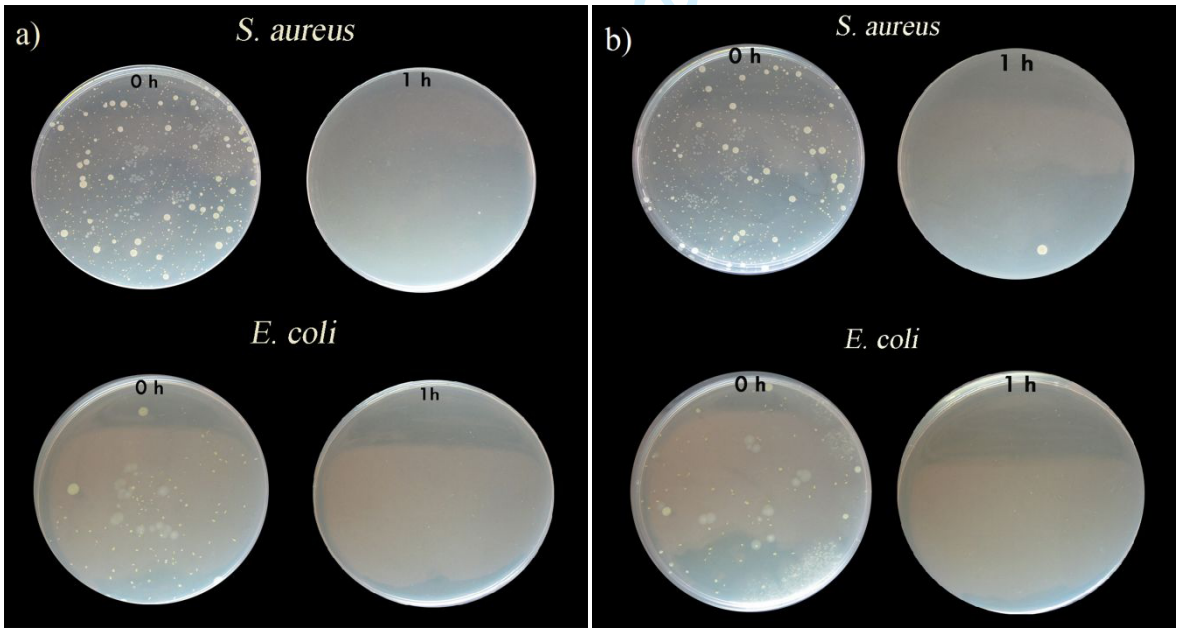

Fig. 9. Photographs of *S. aureus* TL and *E. coli* ATCC25922 colonies remaining before incubation and after 1 h of incubation with for a) 0.25Ag/PVA and b) 0.25Ag/PVA/Gr hydrogels

CONCLUSION

In this work, we have synthesized silver nanoparticles, as a green and efficient antibacterial agent, directly inside the poly(vinyl alcohol)-based hydrogel matrices, following the electrochemical in situ reduction method. The efficient incorporation and stabilization of AgNPs inside the polymer matrices was confirmed by UV-visible spectroscopy and FE-SEM, which confirmed the nano-sized diameters around 40-60 nm. Moreover, the stabilization is achieved via the interactions between AgNPs and certain functional groups on polymer chains, such as –OH, as shown by Raman and FTIR spectroscopies. Thermal stability was improved by the presence of both AgNPs and graphene, as confirmed by DSC. The silver release profiles were monitored for 28 days in the modified phosphate buffered solution at 37 ºC, and the obtained profiles exhibited characteristic burst release effect in the initial period. The in-depth silver release analysis was carried out by fitting with several theoretical models that confirmed the predominantly diffusion-controlled mechanism of release. Finally, antibacterial tests confirmed strong antibacterial activity of both Ag/PVA and Ag/PVA/Gr within 24 h, indicating excellent potential for wound dressing applications.

Acknowledgements**:** This work was supported by the Ministry of Education, Science and Technological Development of the Republic of Serbia (Contracts No. 451-03-9/2021-14/200135 and 451-03-9/2021-14/200287). The authors also wish to acknowledge the funding from the European Union's Horizon 2020 research and innovation programme under grant agreement No. 952033.

REFERENCES

[1] J. S. Boateng, K. H. Matthews, H. N. E. Stevens, G. M. Eccleston, *J. Pharm. Sci.* **2008**, *97*, 2892. https://doi.org/10.1002/jps.

[2] A. Bianchera, O. Catanzano, J. Boateng, L. Elviri, The Place of Biomaterials in Wound Healing, in J. Boateng (Ed.), *Therapeutic Dressings and Wound Healing Applications*, John Wiley and Sons Ltd, London, **2020**, pp. 337. https://doi.org/10.1002/9781119433316.ch15.

[3] R. C. Opt Veld, X. F. Walboomers, J. A. Jansen, F. A. D. T. G. Wagener, *Tissue Eng. - Part B Rev.* **2020**, *26*, 230. https://doi.org/10.1089/ten.teb.2019.0281.

[4] A. Karimi, W. M. A. Wan Daud, *Polym. Compos.* **2017**, *38*, 1135. https://doi.org/10.1002/pc.23676.

[5] R. Surudžić, A. Janković, M. Mitrić, I. Matić, Z. D. Juranić, L. Živković, V. Mišković-Stanković, K. Y. Rhee, S. J. Park, D. Hui, *J. Ind. Eng. Chem.* **2016**, *34*, 250. https://doi.org/10.1016/j.jiec.2015.11.016.

[6] J. Jose, M. A. Al-Harthi, M. A. A. AlMa'adeed, J. B. Dakua, S. K. De, *J. Appl. Polym. Sci.* **2015**, *132*, 1. https://doi.org/10.1002/app.41827.

[7] J. Wang, X. Wang, C. Xu, M. Zhang, X. Shang, *Polym. Int.* **2011**, *60*, 816. https://doi.org/10.1002/pi.3025.

[8] C. Shi, C. Wang, H. Liu, Q. Li, R. Li, Y. Zhang, Y. Liu, Y. Shao, J. Wang, *Front. Bioeng. Biotechnol.* **2020**, *8*, 1. https://doi.org/10.3389/fbioe.2020.00182.

[9] C. Liao, Y. Li, S. C. Tjong, *Int. J. Mol. Sci.* **2019**, *20*, 1. https://doi.org/10.3390/ijms20020449.

[10] R. Surudžić, A. Janković, N. Bibić, M. Vukašinović-Sekulić, A. Perić-Grujić, V. Mišković-Stanković, S. J. Park, K. Y. Rhee, *Compos. Part B-Eng.* **2016**, *85*, 102. https://doi.org/10.1016/j.compositesb.2015.09.029.
[11] J. Krstić, J. Spasojević, A. Radosavljević, A. Perić-Grujić, M. Đurić, Z. Kačarević-Popović, S. Popović, *J. Appl. Polym. Sci.* **2014**, *2014*, 40321. https://doi.org/10.1002/app.40321.
[12] M. M. Abudabbus, I. Jevremović, A. Janković, A. Perić-Grujić, I. Matić, M. Vukašinović-Sekulić, D. Hui, K. Y. Rhee, V. Mišković-Stanković, *Compos. Part B-Eng.* **2016**, *104*, 26. https://doi.org/10.1016/j.compositesb.2016.08.024.
[13] M. M. Abudabbus, I. Jevremović, K. Nešović, A. Perić-Grujić, K. Y. Rhee, V. Mišković-Stanković, *Compos. Part B-Eng.* **2018**, *140*, 99. https://doi.org/10.1016/j.compositesb.2017.12.017.
[14] K. Nešović, M. M. Abudabbus, K. Y. Rhee, V. Mišković-Stanković, *Croat. Chem. Acta* **2017**, *90*, 207. https://doi.org/10.5562/cca3133.
[15] D. Pencheva, R. Bryaskova, T. Kantardjiev, *Mater. Sci. Eng., C* **2012**, *32*, 2048.
[16] K. H. Mahmoud, *Spectrochim. Acta. A. Mol. Biomol. Spectrosc.* **2015**, *138*, 434. https://doi.org/10.1016/j.saa.2014.11.074.
[17] K. Nešović, V. Mišković-Stanković, *Polym. Eng. Sci.* **2020**, *60*, 1393. https://doi.org/10.1002/pen.25410.
[18] A. N. Ananth, S. C. G. K. Daniel, T. A. Sironmani, S. Umapathi, *Colloid. Surface. B* **2011**, *85*, 138. https://doi.org/10.1016/j.colsurfb.2011.02.012.
[19] A. Chaturvedi, A. K. Bajpai, J. Bajpai, *Polym. Compos.* **2015**, *36*, 1983. https://doi.org/10.1002/pc.23108.
[20] J. Krstić, J. Spasojević, A. Radosavljević, M. Šiljegović, Z. Kačarević-Popović, *Radiat. Phys. Chem.* **2014**, *96*, 158. https://doi.org/10.1016/j.radphyschem.2013.09.013.
[21] S. K. Bajpai, N. Chand, M. Mahendra, *Polym. Eng. Sci.* **2013**, *53*, 1751. https://doi.org/10.1002/pen23424.
[22] M. Bandla, B. R. Abbavaram, V. Kokkarachedu, R. E. Sadiku, *Polym. Compos.* **2017**, *38*, E16. https://doi.org/10.1002/pc.23963.
[23] A. Sionkowska, M. Walczak, M. Michalska-Sionkowska, *Polym. Compos.* **2020**, *41*, 951. https://doi.org/10.1002/pc.25426.
[24] P. P. Das, V. Chaudhary, F. Ahmad, A. Manral, *Polym. Compos.* **2021**, *42*, 2152. https://doi.org/10.1002/pc.25968.
[25] G. Chitra, D. S. Franklin, S. Sudarsan, M. Sakthivel, S. Guhanathan, *Polym. Eng. Sci.* **2018**, *58*, 2133. https://doi.org/10.1002/pen.24824.
[26] S. Zhang, Y. Tang, B. Vlahovic, *Nanoscale Res. Lett.* **2016**, *11*, 1. https://doi.org/10.1186/s11671-016-1286-z.
[27] Ž. Jovanović, A. Radosavljević, M. Šiljegović, N. Bibić, V. Mišković-Stanković, Z. Kačarević-Popovic, *Radiat. Phys. Chem.* **2012**, *81*, 1720. https://doi.org/10.1016/j.radphyschem.2012.05.019.
[28] Z. Jovanovic, A. Radosavljevic, J. Stojkovska, B. Nikolic, B. Obradovic, Z. Kacarevic-Popovic, V. Miskovic-Stankovic, *Polym. Compos.* **2014**, *35*, 217. https://doi.org/10.1002/pc.22653.
[29] J. Helmlinger, C. Sengstock, C. Groß-Heitfeld, C. Mayer, T. A. Schildhauer, M. Köller, M. Epple, *RSC Adv.* **2016**, *6*, 18490. https://doi.org/10.1039/c5ra27836h.
[30] Ž. Jovanović, A. Radosavljević, Z. Kačarević-Popović, J. Stojkovska, A. Perić-Grujić, M. Ristić, I. Z. Matić, Z. D. Juranić, B. Obradovic, V. Mišković-Stankovic, *Colloid. Surface. B* **2013**, *105*, 230. https://doi.org/10.1016/j.colsurfb.2012.12.055.

[31] K. Nešović, A. Janković, V. Kojić, M. Vukašinović-Sekulić, A. Perić-Grujić, K. Y. Rhee, V. Mišković-Stanković, *Compos. Part B-Eng.* **2018**, *154*, 175. https://doi.org/10.1016/j.compositesb.2018.08.005.
[32] K. Nešović, A. Janković, T. Radetić, M. Vukašinović-Sekulić, V. Kojić, L. Živković, A. Perić-Grujić, K. Y. Rhee, V. Mišković-Stanković, *Eur. Polym. J.* **2019**, *121*, 109257. https://doi.org/10.1016/j.eurpolymj.2019.109257.
[33] K. Nešović, A. Janković, A. Perić-Grujić, M. Vukašinović-Sekulić, T. Radetić, L. Živković, S. J. Park, K. Yop Rhee, V. Mišković-Stanković, *J. Ind. Eng. Chem.* **2019**, *77*, 83. https://doi.org/10.1016/j.jiec.2019.04.022.
[34] G. S. El-Feky, S. S. Sharaf, A. El Shafei, A. A. Hegazy, *Carbohydr. Polym.* **2017**, *158*, 11. https://doi.org/10.1016/j.carbpol.2016.11.054.
[35] S. Hosseinzadeh, H. Hosseinzadeh, S. Pashaei, *Polym. Compos.* **2019**, *40*, E559. https://doi.org/10.1002/pc.24875.
[36] X. Huang, C. S. Brazel, *J. Control. Release* **2001**, *73*, 121. https://doi.org/10.1016/S0168-3659(01)00248-6.
[37] H. Kim, R. Fassihi, *J. Pharm. Sci.* **1997**, *86*, 323. https://doi.org/10.1021/js960307p.
[38] L. Serra, J. Doménech, N. A. Peppas, *Biomaterials* **2006**, *27*, 5440. https://doi.org/10.1016/j.biomaterials.2006.06.011.
[39] E. Fages, J. Pascual, O. Fenollar, D. Garcia-Sanoguera, R. Balart, *Polym. Eng. Sci.* **2011**, *51*, 804. https://doi.org/10.1002/pen21889.
[40] M. S. Rubina, E. E. Said-Galiev, A. V. Naumkin, A. V. Shulenina, O. A. Belyakova, A. Y. Vasil'kov, *Polym. Eng. Sci.* **2019**, *59*, 2479. https://doi.org/10.1002/pen.25122.
[41] R. W. Korsmeyer, R. Gurny, E. Doelker, P. Buri, N. A. Peppas, *Int. J. Pharm.* **1983**, *15*, 25. https://doi.org/10.1016/0378-5173(83)90064-9.
[42] S. Dash, P. N. Murthy, L. Nath, P. Chowdhury, *Acta Pol. Pharm.* **2010**, *67*, 217. https://doi.org/10.1016/S0928-0987(01)00095-1.
[43] T. Higuchi, *J. Pharm. Sci.* **1961**, *50*, 874. https://doi.org/10.1248/cpb.23.3288.
[44] J. Siepmann, N. A. Peppas, *Int. J. Pharm.* **2011**, *418*, 6. https://doi.org/10.1016/j.ijpharm.2011.03.051.
[45] J. Pais, *J. Online Math. Its Appl.* **2001**, *1*. https://www.maa.org/press/periodicals/loci/joma/intuiting-mathematical-objects-using-kinetigrams.
[46] M. C. Makoid, A. Dufour, U. V. Banakar, *S.T.P. Pharma Prat.* **1993**, *3*, 49.
[47] M. Kopcha, N. G. Lordi, K. J. Tojo, *J. Pharm. Pharmacol.* **1991**, *43*, 382. https://doi.org/10.1111/j.2042-7158.1991.tb03493.x.
[48] M. P. Mullarney, T. A. P. Seery, R. A. Weiss, *Polymer.* **2006**, *47*, 3845. https://doi.org/10.1016/j.polymer.2006.03.096.
[49] J. Spasojević, A. Radosavljević, J. Krstić, D. Jovanović, V. Spasojević, M. Kalagasidis-Krušić, Z. Kačarević-Popović, *Eur. Polym. J.* **2015**, *69*, 168. https://doi.org/10.1016/j.eurpolymj.2015.06.008.
[50] P. L. Ritger, N. A. Peppas, *J. Control. Release* **1987**, *5*, 23. https://doi.org/10.1016/0168-3659(87)90034-4.
[51] J. Schindelin, I. Arganda-Carreras, E. Frise, V. Kaynig, M. Longair, T. Pietzsch, S. Preibisch, C. Rueden, S. Saalfeld, B. Schmid, J.-Y. Tinevez, D. J. White, V. Hartenstein, K. Eliceiri, P. Tomancak, A. Cardona, *Nat. Methods* **2012**, *9*, 676. http://dx.doi.org/10.1038/nmeth.2019.
[52] J. Schindelin, C. T. Rueden, M. C. Hiner, K. W. Eliceiri, *Mol. Reprod. Dev.* **2015**, *82*, 518.

https://doi.org/10.1002/mrd.22489.
[53] K. Nešović, A. Janković, T. Radetić, A. P. Grujić, M. V. Sekulić, V. Kojić, K. Y. Rhee, *J. Electrochem. Sci. Eng.* **2020**, *10*, 185. https://doi.org/10.5599/jese.732.
[54] B. Yin, H. Ma, S. Wang, S. Chen, *J. Phys. Chem. B* **2003**, *107*, 8898. https://doi.org/10.1021/jp0349031.
[55] G. Y. Rudko, A. O. Kovalchuk, V. I. Fediv, W. M. Chen, I. A. Buyanova, *J. Colloid Interface Sci.* **2015**, *452*, 33. https://doi.org/10.1016/j.jcis.2015.04.020.
[56] A. Slistan-Grijalva, R. Herrera-Urbina, J. F. Rivas-Silva, M. . Avalos-Borja, F. F. Castillon-Barraza, A. Posada-Amarillas, *Phys. E Low-Dimensional Syst. Nanostructures* **2005**, *27*, 104. https://doi.org/10.1016/j.physe.2004.10.014.
[57] A. Slistan-Grijalva, R. Herrera-Urbina, J. F. Rivas-Silva, M. . Avalos-Borja, F. F. Castillon-Barraza, A. Posada-Amarillas, *Phys. E Low-Dimensional Syst. Nanostructures* **2005**, *25*, 438. https://doi.org/10.1016/j.physe.2004.07.010.
[58] M. Miya, R. Iwamoto, S. Mima, *J. Polym. Sci. Polym. Phys. Ed.* **1984**, *22*, 1149. https://doi.org/10.1002/pol.1984.180220615.
[59] D. Mayo, F. Miller, R. Hannah, *Course Notes On The Interpretation Of Infrared And Raman Spectra*, John Wiley and Sons Ltd, Hoboken, NJ, **2003**.
[60] S. Krimm, C. Y. Liang, G. B. B. M. Sutherland, *J. Polym. Sci.* **1956**, *22*, 227. https://doi.org/10.1016/0022-2852(59)90048-7.
[61] T. Wang, S. Gunasekaran, *J. Appl. Polym. Sci.* **2006**, *101*, 3227. https://doi.org/10.1002/app.23526.
[62] T. Higuchi, *J. Pharm. Sci.* **1963**, *52*, 1145. https://doi.org/10.1002/jps.2600521210.
[63] J. Siepmann, N. A. Peppas, *Adv. Drug Deliv. Rev.* **2001**, *48*, 139. https://doi.org/10.1016/S0169-409X(01)00112-0.

Polymer colloid dispersion

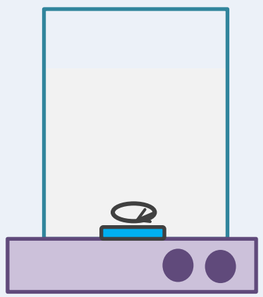

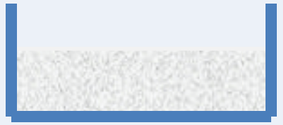

Freezing/thawing cross linking

Cross linked hydrogel disc

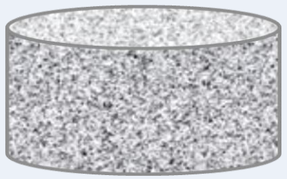

DC power source

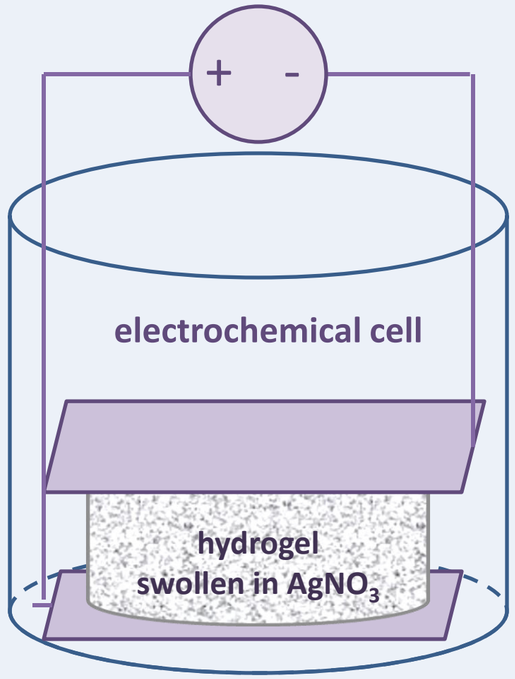

In situ electrochemical synthesis of AgNPs

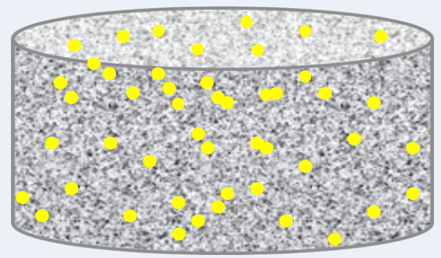

AgNPs-loaded hydrogel

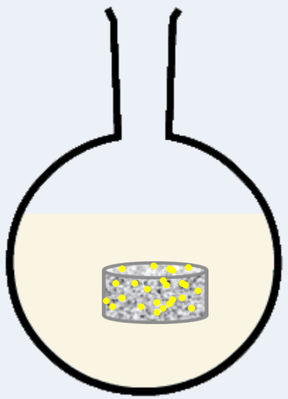

Antibacterial activity

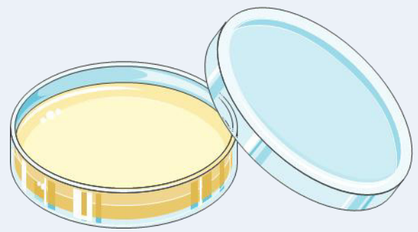

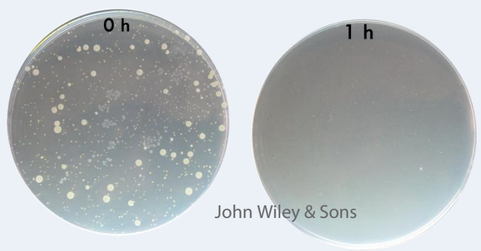

Silver release pH 7.4, 37 °C 28 days

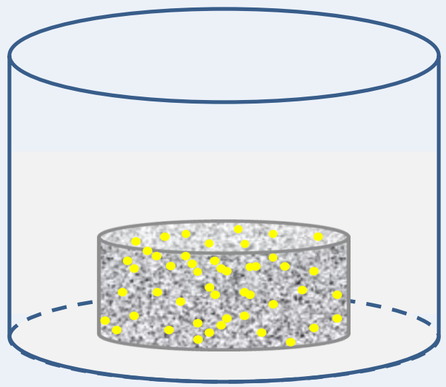

Silver release modeling

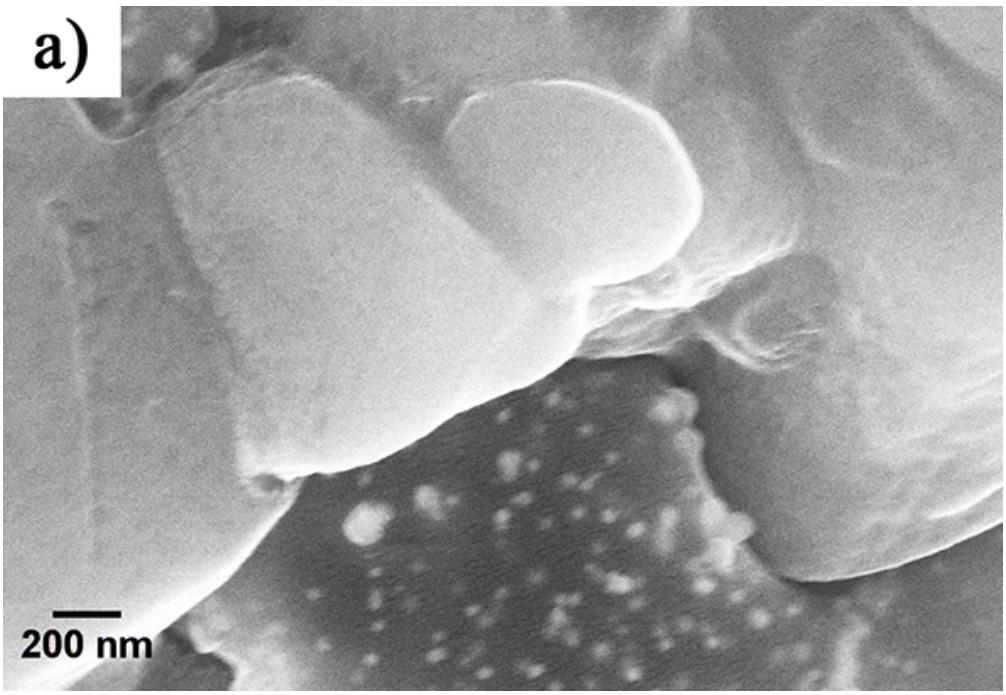

Fig. 1. FE-SEM microphotographs of a) 3.9Ag/PVA and b) 3.9Ag/PVA/Gr hydrogels

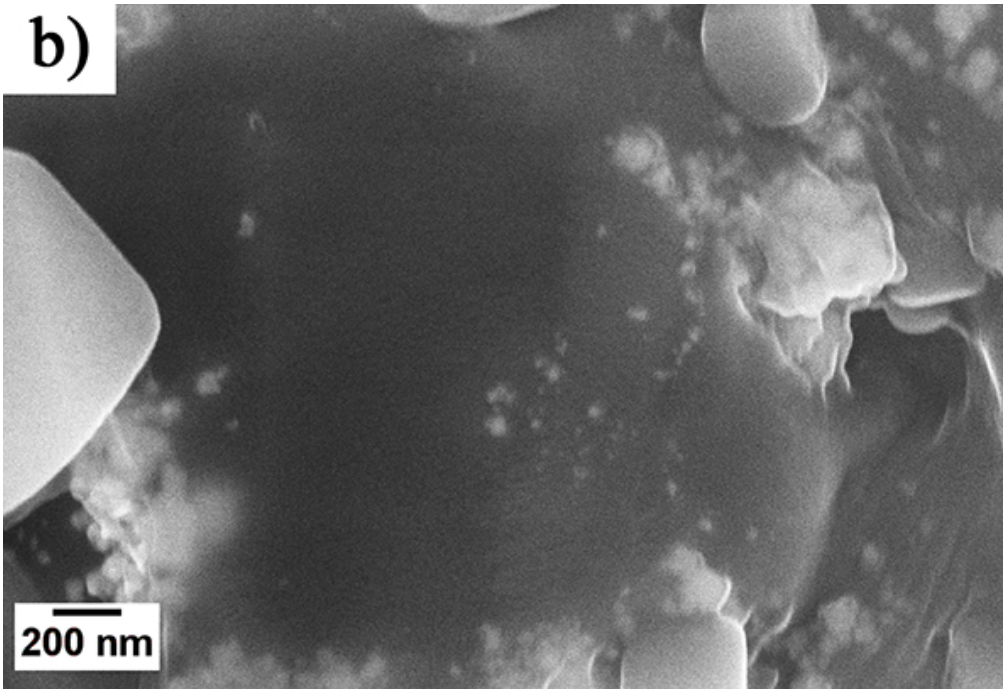

Fig. 1. FE-SEM microphotographs of a) 3.9Ag/PVA and b) 3.9Ag/PVA/Gr hydrogels

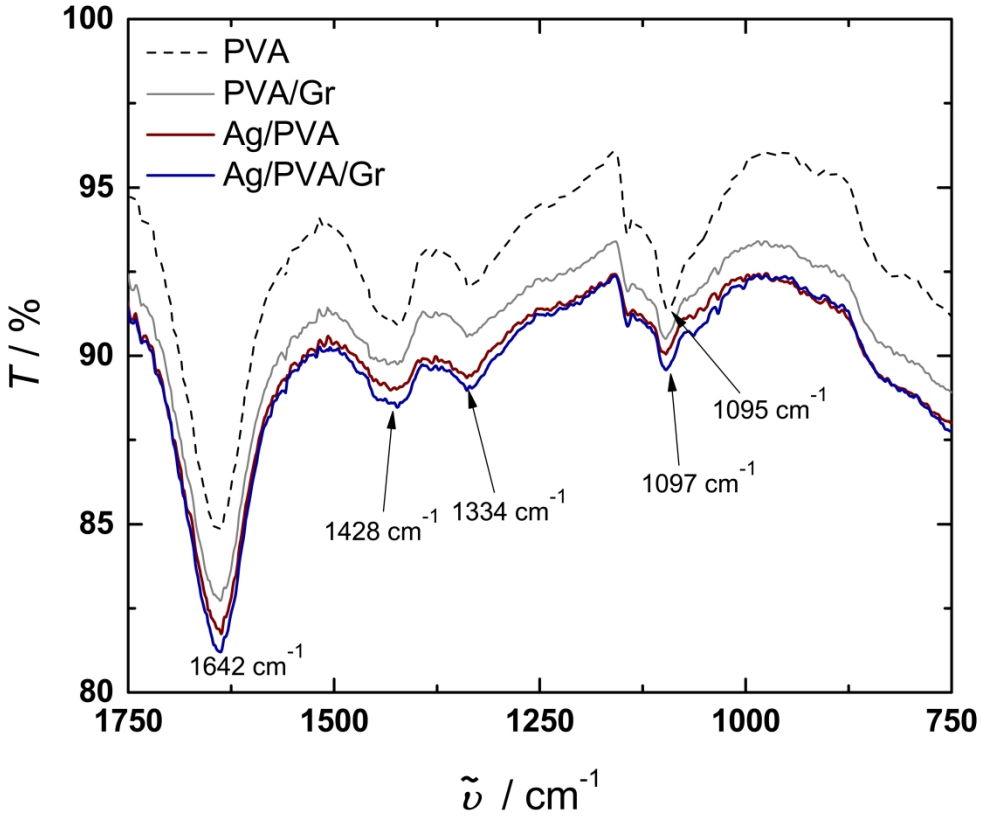

Fig. 2. The fingerprint regions of FT-IR spectra of PVA, PVA/Gr, 3.9Ag/PVA and 3.9Ag/PVA/Gr hydrogels

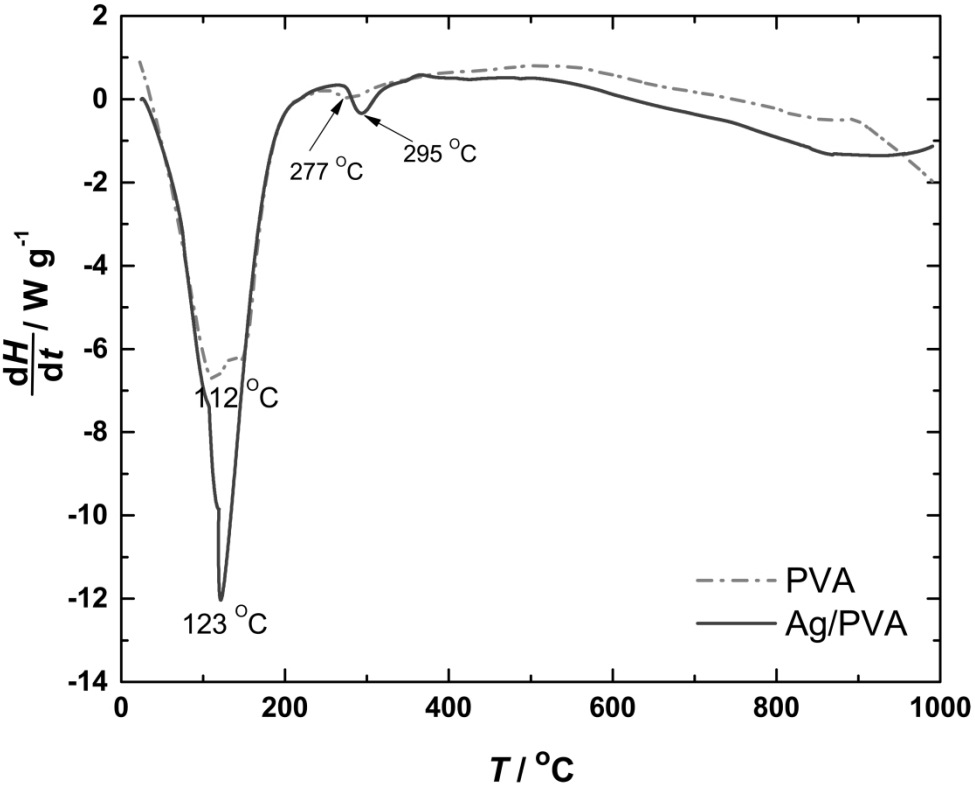

Fig. 3. DSC curves for PVA and 3.9Ag/PVA hydrogels

99x80mm (1000 x 1000 DPI)

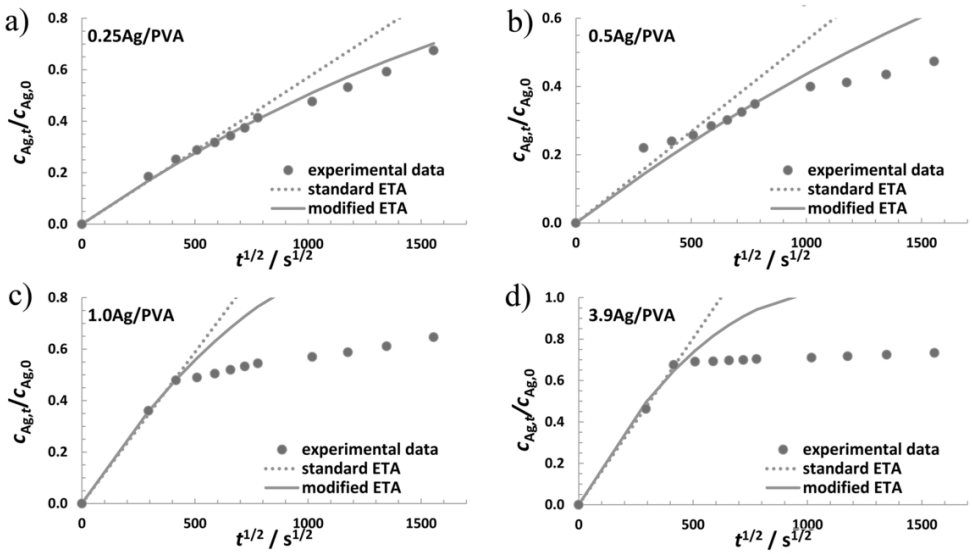

Fig. 4. Early time approximations (ETA) for silver release from a) 0.25Ag/PVA, b) 0.5Ag/PVA, c) 1.0Ag/PVA, and d) 3.9Ag/PVA hydrogels

99x55mm (300 x 300 DPI)

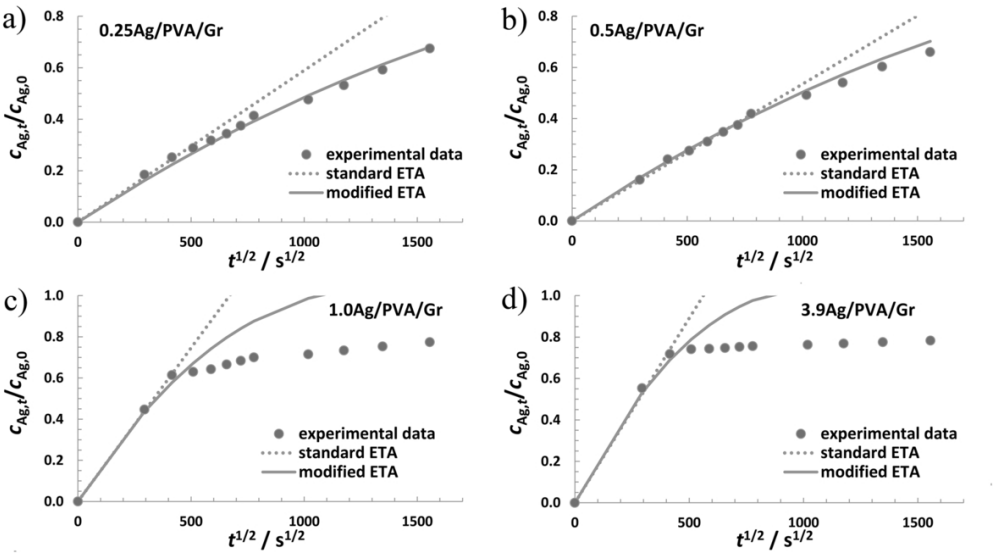

Fig. 5. Early time approximations (ETA) for silver release from a) 0.25Ag/PVA/Gr, b) 0.5Ag/PVA/Gr, c) 1.0Ag/PVA/Gr, and d) 3.9Ag/PVA/Gr hydrogels

99x55mm (300 x 300 DPI)

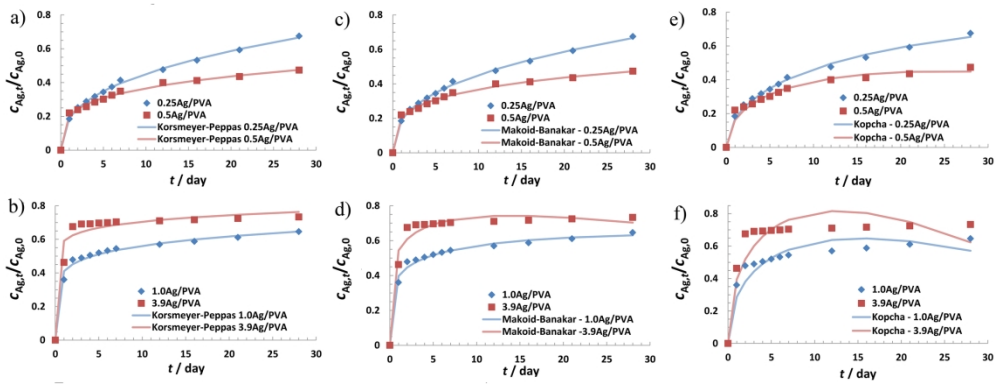

Fig. 6. Models of silver release from 0.25Ag/PVA, 0.5Ag/PVA, 1.0Ag/PVA, and 3.9Ag/PVA hydrogels: a) and b) Korsmeyer-Peppas, c) and d) Makoid-Banakar, e) and f) Kopcha

209x80mm (300 x 300 DPI)

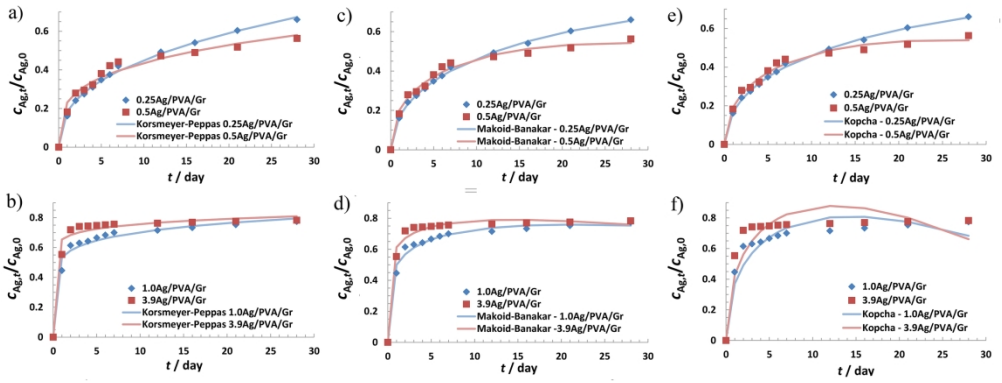

Fig. 7. Models of silver release from 0.25Ag/PVA/Gr, 0.5Ag/PVA/Gr, 1.0Ag/PVA/Gr, and 3.9Ag/PVA/Gr hydrogels: a) and b) Korsmeyer-Peppas, c) and d) Makoid-Banakar, e) and f) Kopcha

209x80mm (300 x 300 DPI)

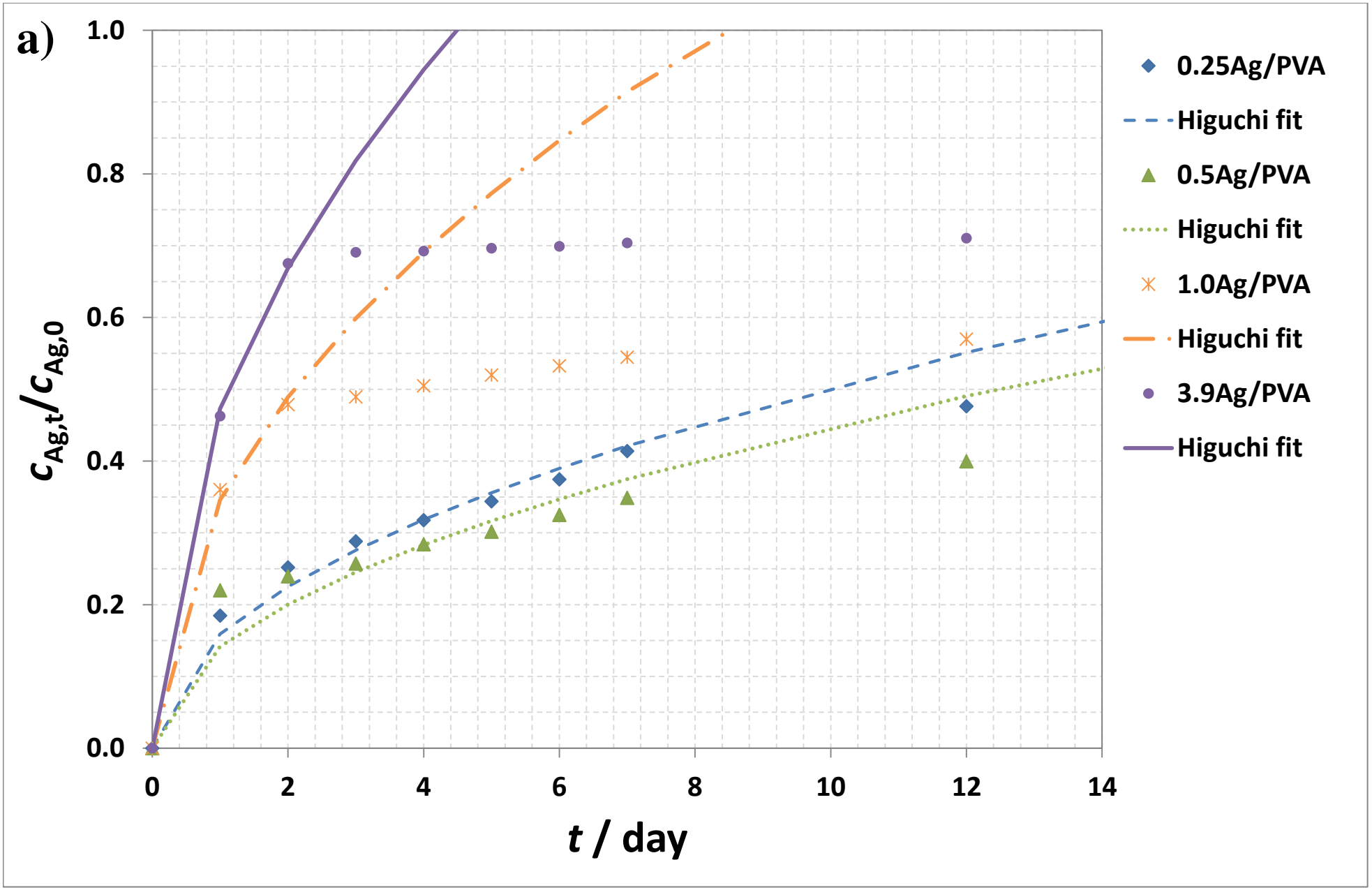
a)
1.0
0.8
0.6
0.4
0.2
0.0
$c_{Ag,t}/c_{Ag,0}$
0
2
4
6
8
10
12
14
t / day
0.25Ag/PVA
Higuchi fit
0.5Ag/PVA
Higuchi fit
1.0Ag/PVA
Higuchi fit
3.9Ag/PVA
Higuchi fit

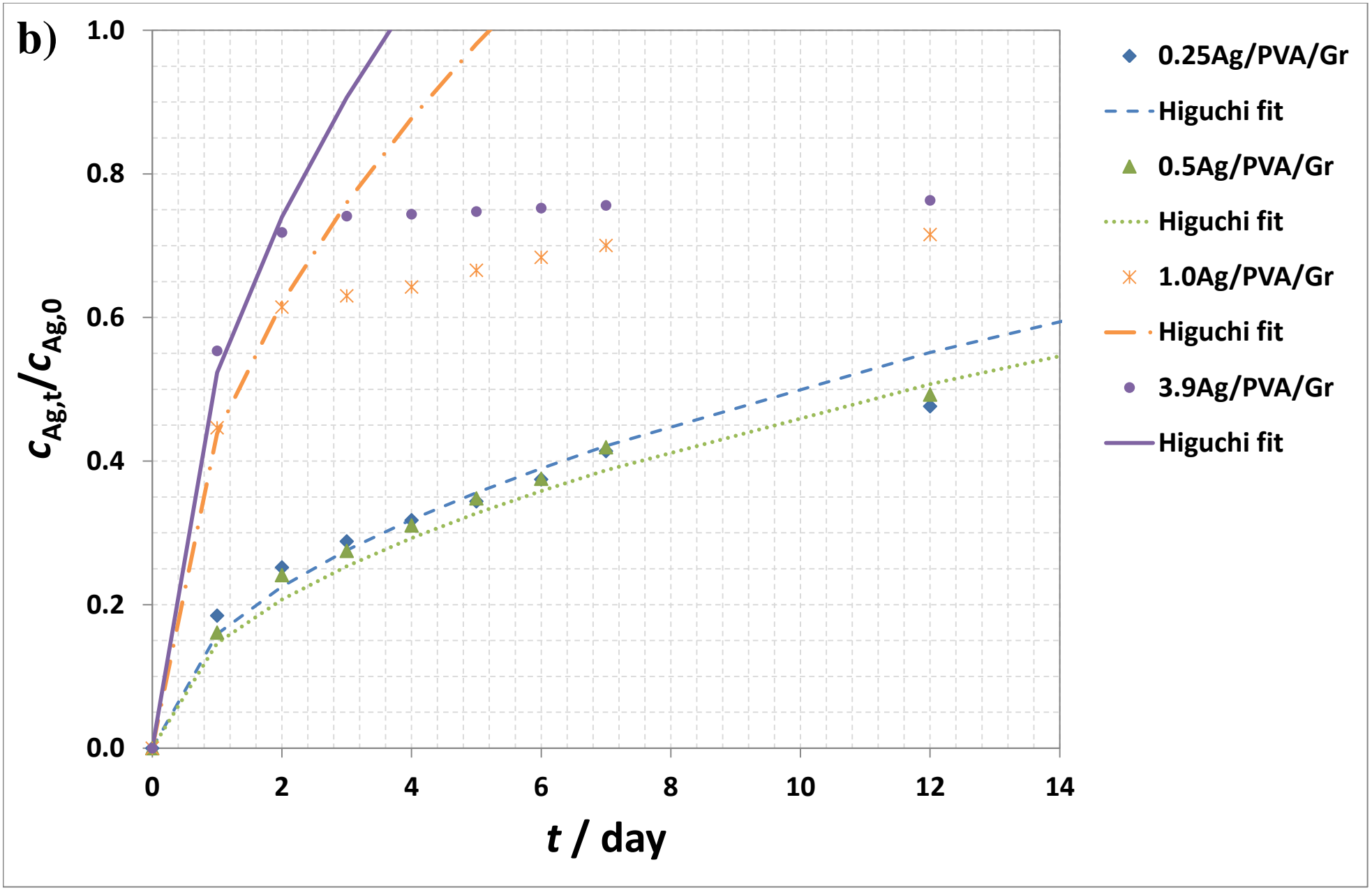
b)
1.0
0.8
0.6
0.4
0.2
0.0
$c_{Ag,t}/c_{Ag,0}$
0
2
4
6
8
10
12
14
t / day
0.25Ag/PVA/Gr
Higuchi fit
0.5Ag/PVA/Gr
Higuchi fit
1.0Ag/PVA/Gr
Higuchi fit
3.9Ag/PVA/Gr
Higuchi fit

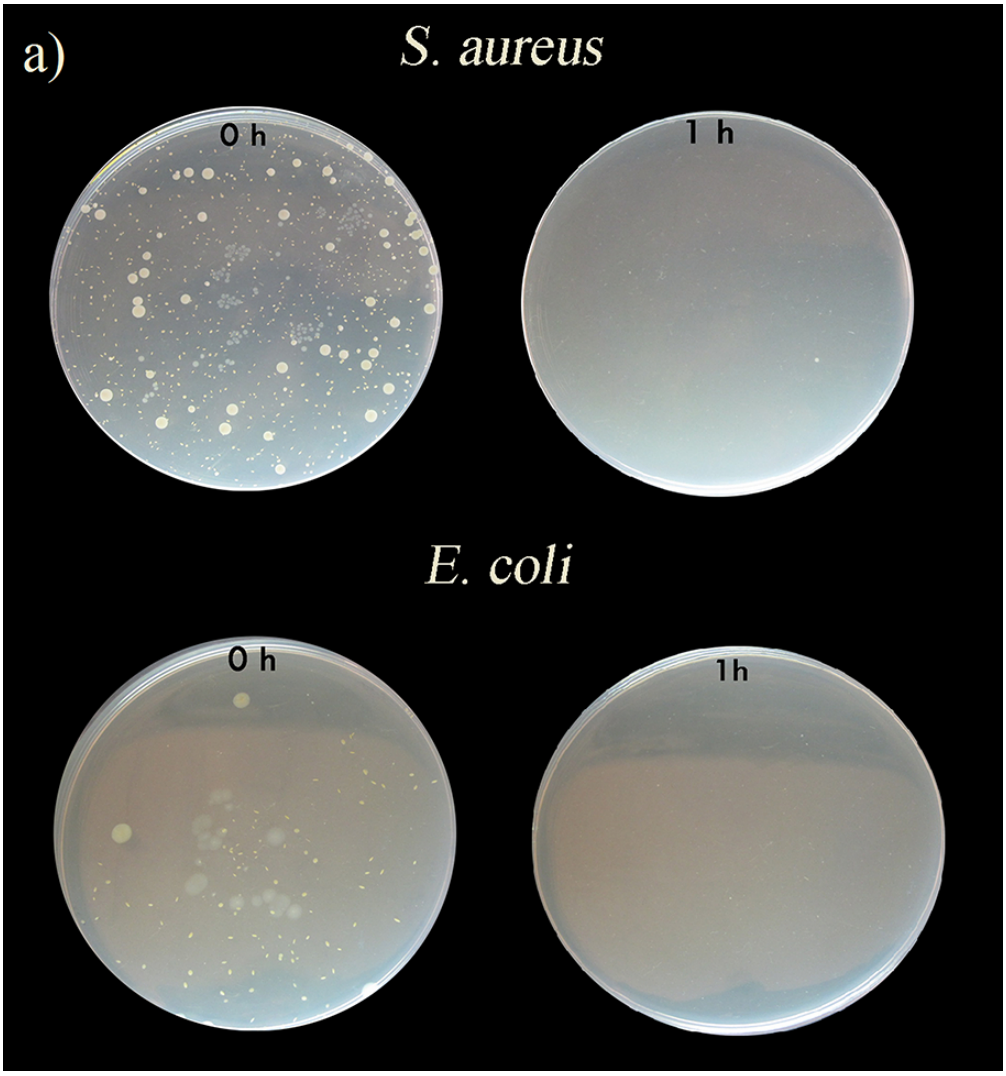

Fig. 9. Photographs of S. aureus TL and E. coli ATCC25922 colonies remaining before incubation and after 1 h of incubation with for a) 0.25Ag/PVA and b) 0.25Ag/PVA/Gr hydrogels

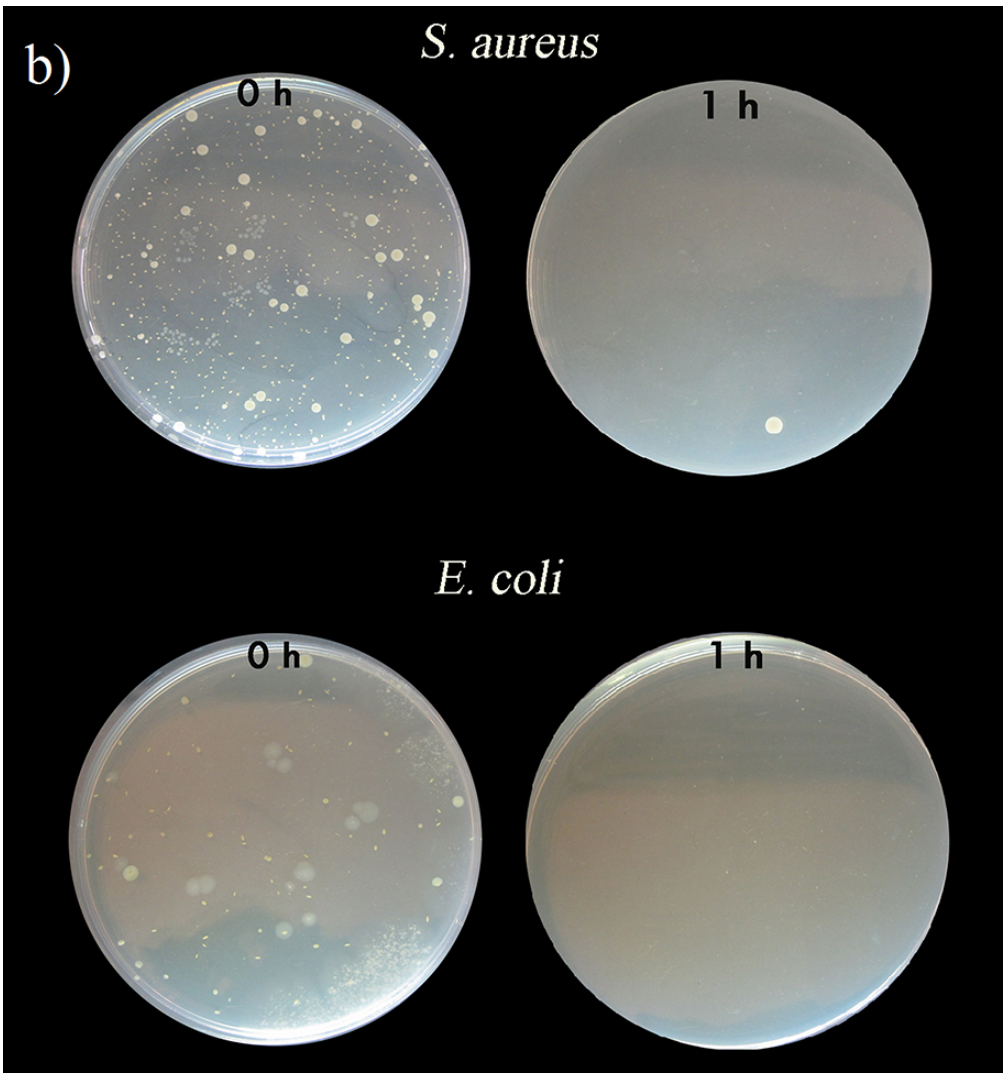

Fig. 9. Photographs of S. aureus TL and E. coli ATCC25922 colonies remaining before incubation and after 1 h of incubation with for a) 0.25Ag/PVA and b) 0.25Ag/PVA/Gr hydrogels